Circulating multimeric immune complexes drive immunopathology in COVID-19

Jakob Ankerhold[1*], Sebastian Giese[1*], Philipp Kolb[1*], Andrea Maul-Pavicic[2], Reinhard E. Voll[2], Nathalie Göppert[1], Kevin Ciminski[1], Clemens Kreutz[4], Achim Lother[5,6], Ulrich Salzer[3], Wolfgang Bildl[7], Tim Welsink[8], Nils G. Morgenthaler[8], Andrea Busse Grawitz[9], Daniela Huzly[1], Martin Schwemmle[1], Hartmut Hengel[1§], Valeria Falcone[1§]

[1]Institute of Virology, Freiburg University Medical Center, Faculty of Medicine, Albert-Ludwigs-University of Freiburg, Freiburg, Germany.
[2]Department of Rheumatology and Clinical Immunology, Freiburg University Medical Center, Faculty of Medicine, Albert-Ludwigs-University of Freiburg, Freiburg, Germany.
[3]Center for Chronic Immunodeficiency (CCI), Freiburg University Medical Center, Faculty of Medicine, Albert-Ludwigs-University of Freiburg, Freiburg, Germany.
[4]Institute of Medical Biometry and Statistics, Freiburg University Medical Center, Faculty of Medicine, Albert-Ludwigs-University of Freiburg, Freiburg, Germany.
[5]Heart Center Freiburg University, Department of Cardiology and Angiology I, Faculty of Medicine, Albert-Ludwigs-University of Freiburg, Freiburg, Germany.
[6]Institute of Experimental and Clinical Pharmacology and Toxicology, Faculty of Medicine, Albert-Ludwigs-University of Freiburg, Freiburg, Germany.
[7]Institute of Physiology II, Faculty of Medicine, Albert-Ludwigs-University of Freiburg, Freiburg, Germany.
[8]InVivo BioTech Services GmbH, Hennigsdorf, Germany.
[9]Institute of Clinical Chemistry and Laboratory Medicine, Faculty of Medicine, Albert-Ludwigs-University of Freiburg, Freiburg, Germany.

[*]contributed equally
[§]corresponding authors

Email: Hartmut.hengel@uniklinik-freiburg.de; valeria.kapper-falcone@uniklinik-freiburg.de

Conflict of interest

The authors declare the following competing financial interest(s): InVivo BioTech Services is a biotechnology company producing antibodies and proteins, including SARS-CoV-2 antigens.

Funding

This work was supported by the Bundesministerium fuer Bildung und Forschung (BMBF) through the Deutsches Zentrum fuer Luft- und Raumfahrt, Germany, (DLR, grant number 01KI2077) and by the Federal State of Baden-Wuerttemberg, Germany, MWK-Sonderfoerdermaßnahme COVID-19/AZ.:33-7533.-6-21/7/2 to M.S.. This work was also supported by an intramural junior investigator fund of the Faculty of Medicine to P.K. (EQUIP - Funding for Medical Scientists, Faculty of Medicine, University of Freiburg) and "NaFoUniMedCovid19" (FKZ: 01KX2021 - COVIM to H.H., FKZ 100493916 B-FAST to H.H.) and DFG HE2526/9-1 to H.H.. RE.V. was funded by DFG research grant TRR130. A.L. is a member of SFB1425, funded by the Deutsche Forschungsgemeinschaft (DFG, German Research Foundation #422681845). The funders had no role in the study design, data analysis, data interpretation, and in the writing of this report. All authors had full access to the data in the study and accept responsibility to submit for publication.

Graphical abstract

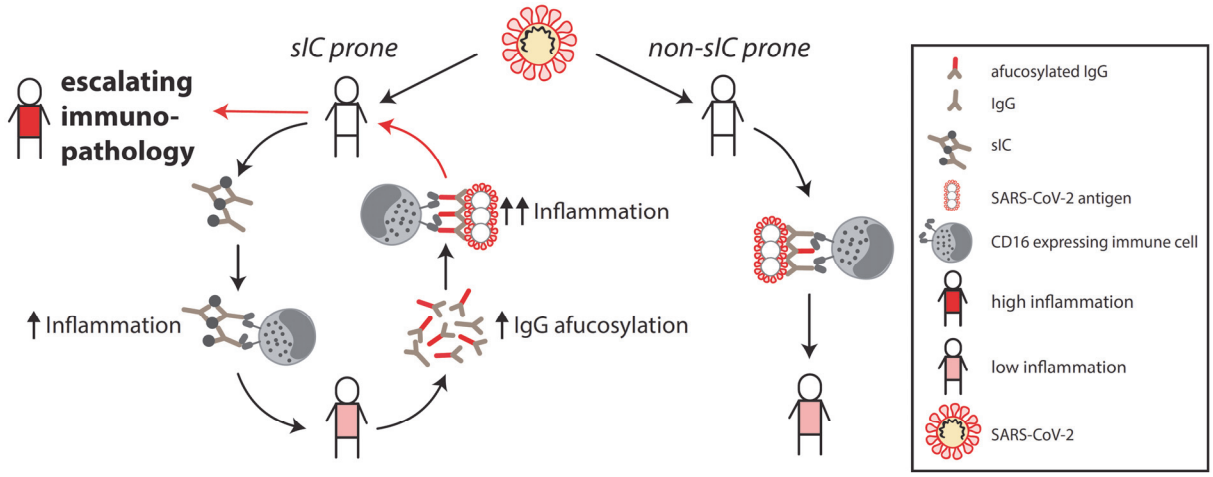

A vicious cycle of immunopathology in COVID-19 patients is driven by soluble multimeric immune complexes (sICs). SARS-CoV-2 infection triggers sIC formation in prone individuals. Activation of FcγRIII/CD16 expressing immune cells by sICs precedes a humoral response to SARS-CoV2 infection. sICs and infection add to IgG afucosylation, further enhancing FcγRIII/CD16 activation by opsonized targets. High inflammation induces further sIC mediated immune cell activation ultimately leading to an escalating immunopathology.

Abstract

A dysregulated immune response with high levels of SARS-CoV-2 specific IgG antibodies characterizes patients with severe or critical COVID-19. Although a robust IgG response is traditionally considered to be protective, excessive triggering of activating Fc-gamma-receptors (FcγRs) could be detrimental and cause immunopathology. Here, we document that patients who develop soluble circulating IgG immune complexes (sICs) during infection are subject to enhanced immunopathology driven by FcγR activation. Utilizing cell-based reporter systems we provide evidence that sICs are predominantly formed prior to a specific humoral response against SARS-CoV-2. sIC formation, together with increased afucosylation of SARS-CoV-2 specific IgG eventually leads to an enhanced CD16 (FcγRIII) activation of immune cells reaching activation levels comparable active systemic lupus erythematosus (SLE) disease. Our data suggest a vicious cycle of escalating immunopathology driven by an early formation of sICs in predisposed patients. These findings reconcile the seemingly paradoxical findings of high antiviral IgG responses and systemic immune dysregulation in severe COVID-19.

Keywords

Soluble immune complexes (sICs), Fcγ receptors, COVID-19, inflammation, immunopathology

Clinical implications

The identification of sICs as drivers of an escalating immunopathology in predisposed patients opens new avenues regarding intervention strategies to alleviate critical COVID-19 progression.

Introduction

Since the emergence of SARS-CoV-2 in late December 2019 (1), more than 199 million laboratory confirmed infections (as of August 3rd, 2021) have been reported, with cases continuously rising (2). Accordingly, rapid insights into the disease manifestations and pathogenesis have been globally obtained. A hallmark of the coronavirus disease 2019 (COVID-19) is a respiratory infection which can progress to an acute respiratory distress syndrome (ARDS). Next to asymptomatic infections, COVID-19 symptoms differ widely according to the disease process and may comprise fever, coughing, pneumonia, dyspnea, hypoxia and lymphopenia (3). While fever and coughing are common symptoms, pneumonia, hypoxia, dyspnea, certain organ manifestations and lymphopenia indicate critical or fatal infections (3-6). Pronounced dyspnea can eventually progress to ARDS, a severe complication frequently observed in critically ill patients (7, 8). Although overall disease severity and in particular breathing difficulties are related to viral load (9), age (4, 10-13) and underlying medical conditions (4, 11, 12), the delayed kinetics of respiratory failure strongly suggest an essential role of the host immune response (3, 11). Typically, aggravation occurs between 9-11 days after symptom onset (12) and correlates with high levels of SARS-CoV-2 specific IgG antibodies and systemic effects of pro-inflammatory cytokines such as IL-6 and TNFα (3, 14-16). This cytokine release, primarily the result of macrophage and T helper (T_H) cell activation (17), includes pattern recognition receptor (PRR) signaling in the context of innate immunity but can also occur by Fcγ receptor (FcγR) activation (18). Triggered by immune complexes (antibody-antigen complex), the cytokine release following FcγR activation represents a potent defense mechanism against invading pathogens. A prototypical activating FcγR in this regard is FcγRIII (CD16) expressed by NK cells (19, 20), monocyte-derived macrophages (CD16A) (21) or neutrophils (CD16B, 98% sequence identical ectodomains). Specifically, CD16 is able to sense circulating soluble immune complexes (sICs) as they are formed in certain autoimmune diseases such as systemic lupus erythematosus (SLE) (22-25) and viral infections (26). Overstimulation of activating FcγRs in these cases is associated with disease severity (26-28) and thus an FcγR-driven overshooting inflammatory response (18) might be an explanation for the pronounced immunopathology observed during severe courses of COVID-19 (29). Consistently, hyper-inflammation in SARS-CoV-1 and MERS infected patients has been previously proposed as a possible pathogenic factor (30) and could be demonstrated in mice and macaques infected with SARS-CoV-1 (31, 32). Furthermore, N297-dependent glycan-modifications such as afucosylation within the constant region of IgG antibodies are known to enhance FcγR binding, in turn promoting inflammation. It has been shown that enhanced FcγRIII activation by low-fucosylated anti-SARS-CoV-2-S IgG leads to excessive alveolar macrophage activation, driving severe COVID-19 disease progression (33). Further, it has been proposed that uncleared antigen-antibody immune complexes (ICs) might be involved in the pathogenesis of severe disease leading to systemic complement activation and tissue damage, neutrophil activation, cytokine storm, systemic vasculitis, microvascular thrombosis and organ failure (34-39). However, comprehensive evidence that circulating sICs impact disease progression is still missing. Here, we aimed to further delineate the contribution of IgG-mediated effector functions regarding COVID-19 severity in patient cohorts with varying disease progressions. This revealed a marked correlation between CD16 activation by patient IgG and severity of disease. Additionally, we identified circulating CD16-reactive sICs to be abundantly present in the serum of patients with critical and severe disease, but not in the serum of patients with a mild disease. sIC levels were comparable to those found in SLE patients with active disease. As sIC formation preceded a SARS-CoV-2 specific humoral response in most cases, we conclude that a so far undisclosed predisposing condition divides patients into sIC-prone and non-sIC-prone individuals with patients developing sICs in response to an infectious trigger also developing enhanced disease. Our data suggest a vicious cycle leading to an

138 escalating immunopathology driven by the early formation of sICs. Our findings enable new
139 avenues of intervention against COVID-19 and highly warrant further investigation into the
140 origin and composition of sICs predisposing to COVID-19 disease.
141
142
143 **Materials and Methods**
144
145 **Subjects and specimens**
146 Between March 2020 and April 2020, 41 patients with SARS-CoV-2 infection confirmed by
147 real-time PCR were hospitalized in the University Medical Center, Freiburg. Serum samples
148 were collected during hospitalization for routine laboratory testing. Clinical data were obtained
149 from electronic medical records. A total of 27 patients necessitating invasive mechanical
150 ventilation were included in the critical group. Fourteen patients requiring O_2 supplementation
151 were included in the severe group. Additionally, serum samples from 29 mild COVID-19 cases
152 and 30 healthy donor (HD) plasma samples were used as controls in this study. For the SLE
153 patient control cohort, sera were obtained from the Immunologic, Rheumatologic Biobank (IR-
154 B) of the Department of Rheumatology and Clinical Immunology.
155
156 **Cell culture**
157 African green monkey kidney Vero E6 cells (ATCC CRL-1586) were cultured at 37°C in
158 Dulbecco's Modified Eagle Medium (DMEM) supplemented with 10% (vol/vol) fetal calf
159 serum (FCS, Biochrom), sodium pyruvate (1x, Gibco) and 100 U/ml penicillin-Streptomycin
160 (Gibco). BW5147 mouse thymoma cells (BW, obtained from ATCC: TIB-47) were stably
161 transduced with human FcγR as previously described (40, 41). Cells were maintained at $3x10^5$
162 to $9x10^5$ cells/ml in Roswell Park Memorial Institute medium (RPMI GlutaMAX, Gibco)
163 supplemented with 10% (vol/vol) FCS, sodium pyruvate (1x, Gibco), 100 U/ml penicillin-
164 Streptomycin (Gibco) β-mercaptoethanol (0.1 mM, Gibco). Cells were cultured at 37°C, 5%
165 CO_2. All cell lines were routinely tested for mycoplasma.
166
167 **Monitoring of antibody response to SARS-CoV-2 by ELISA**
168 Serum IgG antibody titers targeting S1- and N-SARS-CoV-2 proteins were measured using
169 commercial enzyme-linked immunosorbent assay (ELISA). Anti-S1- SARS-CoV-2 IgG was
170 measured by the anti-SARS-CoV-2 ELISA (IgG) Euroimmune Kit (Euroimmune, Lübeck,
171 Germany) according to manufacturer's protocol. Results, expressed as arbitrary units (AU),
172 were evaluated semi-quantitatively by calculation of the ratio of the extinction of the control or
173 patient sample over the extinction of the calibrator. This ratio is interpreted as follows: < 0.8
174 negative; ≥ 0.8 to <1.0 borderline; ≥ 1.1 positive. Anti-N SARS-CoV-2 IgG was detected using
175 the recomWell SARS-CoV-2 IgG Kit (Mikrogen Diagnostik GmbH, Neuried, Germany)
176 according to manufacturer's protocol. The corresponding antibody activity expressed in AU/ml
177 is calculated using the formula (absorbance of sample / absorbance of cut-off) × 20. Results are
178 interpreted as follow: < 20 negative; ≥ 20 to < 24 borderline; > 24 positive. IgG against the
179 SARS-CoV-2 Spike Glycoprotein Receptor Binding Domain (RBD) were detected using
180 SARS-CoV-2 IgG ELISA Reagent Set, kindly provided by InVivo (InVivo Biotech Services
181 GmbH, Hennigsdorf, Germany) according to manufacturer's protocol.
182
183 **Fcγ receptor activation assay**
184 FcγRIIIA (CD16A, 158V) activation was measured by a cell-based assay as previously
185 described (42). For detection of anti-S and anti-RBD-specific FcγR activation we utilized
186 SARS-CoV-2-S- and RBD-coated plates (kindly provided by InVivo Biotech Services GmbH,
187 Hennigsdorf, Germany). The recombinant (S)-protein was produced under serum-free
188 conditions in mammalian cells and contains amino acid residues 1 to 1213 of the SARS-CoV-

2 Wuhan-Hu-1-isolate (GenBank annotation QHD43416.1). The furin cleavage site was mutated, two mutations for protein stabilization were included, and the C-terminal domain was replaced by a T4 trimerization sequence and a C-terminal hexa-His-Tag (43). The recombinant RBD-protein represented amino acids 319 to 541 of the (S)-protein mentioned before. Both recombinant proteins were purified using immobilized metal exchange chromatography (IMAC) and preparative SEC under standard conditions in a regulated environment. Microtiter plates were coated using 0.2 µg recombinant (S)-protein or RBD-protein per well. N-specific FcγR activation was determined using plates coated with SARS-CoV-2-N (Mikrogen Diagnostik GmbH, Neuried, Germany). Respective plates were subsequently incubated with serial dilutions of SARS-CoV-2 positive sera or control sera in RPMI supplemented with 10% (vol/vol) FCS for 30 min at 37°C. All wells were thoroughly washed before co-cultivation with BW5147 reporter cells for 16 h at 37°C, 5% CO_2. Cross-link activation of reporter cells was performed by direct coating of target antibody to ELISA plate (Nunc Maxisorp; 96 well, flat transparent), followed by a blocking step and incubation with 2×10^5 reporter cells per well. For all activation assays, mouse IL-2 secretion was quantified by anti-IL-2 ELISA, as described earlier. FcγRIIIA (CD16A) activation by multimeric sICs was measured by a recently developed cell-based assay (25, 44). Briefly, $2x10^5$ BW5147-CD16 reporter cells were incubated with SARS-CoV-2 sera in a total volume of 200 µl for 16 h at 37°C, 5% CO_2. Incubation was performed in a 96-well ELISA plate (Nunc Maxisorp) pre-treated with PBS containing10% FCS for 1 h at 4°C to avoid direct binding of serum IgG to the plate. Reporter cell mIL-2 secretion was quantified via ELISA as described previously (42).

Purification of SARS-CoV2-S and –N specific antibodies from serum

SARS-CoV-2-specific antibodies were purified using SARS-CoV-2 spike protein (S)-coated plates (kindly provided by InVivo BioTech Services) and - nucleocapsid (N) - coated plates recomWell SARS-CoV-2 IgG (Mikrogen Diagnostik GmbH, Neuried, Germany). Patient sera were diluted 1:5 in 100 µl (two wells per serum sample) and incubated for one hour at 37°C with the S- and N-precoated plates. After washing using PBS-T (0.05% Tween 20) 100 mM formic acid (30 µl/well) was added and incubated for 5 min on an orbital shaker at room temperature (RT) to elute bound IgG. Following pH neutralization using TRIS buffer (1 M), the eluates were either directly processed or stored at 4°C.

Quantitation of antigen-specific IgG amount

In order to determine the relative S1- and N-SARS-CoV-2 specific IgG antibody concentration of the generated eluates, S1- and N-ELISA were performed by the anti-SARS-CoV-2 ELISA (IgG) Euroimmune Kit (Euroimmune, Lübeck, Germany) and anti-N SARS-CoV-2 IgG ELISA (recomWell SARS-CoV-2 IgG Kit (Mikrogen Diagnostik GmbH, Neuried, Germany) as aformentioned.

Analysis of antigen-specific IgG-Fc fucosylation

Fucosylation levels of S- and N-specific IgG were measured using a lectin-based ELISA assay. Briefly, 96-well Maxisorb plates (Nunc®) were coated with 50µl/well anti-human IgG-Fab fragment (MyBiosource, MBS674607) at a concentration of 2 µg/ml, diluted in PBS for one hour at 37°C. After three washing steps with PBS-T (0.05% Tween20) unspecific binding sites were blocked adding 300 µl/well Carbo-free™ blocking solution (VectorLab, Inc., SP-5040, LOT: ZF0415) for one hour at room temperature. After three further washing steps, eluted antibodies were serially diluted (2-fold) with PBS in a total volume of 30 µl/well and incubated for one hour at 37°C and 5% CO_2. After washing (3x) using PBS-T, 50 µl/well of 4 µg/ml biotinylated Aleuria Aurantia lectin (AAL, lectin, VectorLab, B-1395) diluted in lectin buffer (10 mM HEPES, 0.1 mM $CaCl_2$, 0.15 M NaCl, 0.1% Tween20) was added and incubated for 45 min at room temperature (RT). Following another three washing steps using PBS-T,

240 Streptavidin-Peroxidase Polymer (Sigma, S 2438), at 1 µg/ml final concentration diluted in
241 LowCross-HRP®-buffer (Candor, Order #.: 200 500) was added and incubated for one hour at
242 RT. After washing five times with PBS-T, 50 µl/well of 1-Step™ Ultra TMB-ELISA Substrate
243 Solution (ThermoFisher, 34028) was applied and the enzyme-substrate reaction was stopped
244 after six minutes using 50 µl/well sulphuric acid (1 M H_2SO_4). Quantification of absorbance,
245 OD_{450nm}, was performed using a Tecan M2000. Relative fucosylation for each generated pool-
246 eluate was calculated by normalizing OD_{450nm} (fucosylation) to its respective relative antigen-
247 specific IgG amount.
248
249 **PEG Precipitation**
250 Sera pools, consisting of eight different sera per pool, were diluted with varying amounts of
251 PEG8000, in order to reach a final PEG8000 concentration of 1, 2, 3.5, 5 and 7.5% respectively.
252 Mixtures were vortexed and incubated overnight at 4°C. For supernatant analysis, precipitates
253 were sedimented via centrifugation at 13.000 rpm for 30 minutes at 4°C. For Mass Spectrometry
254 analysis, PEG8000-precipitated sICs were shortly run into 10% polyacrylamide gels. After
255 over-night fixation (40% ethanol, 10% acetic acid, 50% water) and washing (3x), complete
256 lanes were excised.
257
258 **Benzonase treatment of sera**
259 Serum from six individual patients containing CD16-reactive soluble immune complexes, were
260 treated with 250 units (U) of Benzonase Nuclease (Sigma-Aldrich Chemie GmbH, Munich
261 Germany) for 1 h at 4°C. After treatment, sera were titrated in complete BW5147 culture
262 medium and tested for CD16 reactivity. Non-treated sera served as control. To verify
263 Benzonase activity in the presence of human serum, 3 µg of pIRES-eGFP plasmid DNA
264 (Addgene) were digested with 250 U of Benzonase. Successful nucleic acid digestion was
265 visualized using a 1% agarose gel stained with Midori Green.
266
267 **Immune precipitation**
268 For mass spectrometry analysis of SARS-CoV-2-S specific precipitates, individual sera
269 containing CD16-reactive soluble immune complexes were subjected to immune precipitation
270 (IP) using Pierce MS-compatible magnetic IP kit (ThermoFisher Scientific, Darmstadt,
271 Germany) according to manufacturer's protocol. Briefly 250 µl serum was incubated overnight
272 at 4°C with 5 µg of biotinylated anti-RBD-specific TRES-1-224.2.19 mouse monoclonal
273 antibody or TRES-II-480 (isotype control) (kind gift of H.M. Jäck, Erlangen) before addition
274 of streptavidin magnetic beads. Beads were subsequently collected via centrifugation and
275 elution buffer was added to detach putative precipitated antigen. The elution was dried in a
276 speed vacuum concentrator and shortly run into 10% polyacrylamide gels. After over-night
277 fixation (40% ethanol, 10% acetic acid, 50% water) and washing (3x), complete lanes were
278 excised. Antibody biotinylation was performed using a Pierce antibody biotinylation Kit for IP
279 (ThermoFisher Scientific, Darmstadt, Germany) according to manufacturer's protocol.
280
281 **Mass Spectrometry**
282 Proteins were in-gel digested with sequencing grade modified trypsin (Promega GmbH,
283 Walldorf, Germany) similar to the procedure described by Pandey et al. (45). Vacuum-dried
284 peptides were dissolved in 0.5% trifluoroacetic acid, loaded onto a trap column (C18
285 PepMap100, 5 µm particles, Thermo Fisher Scientific GmbH, Dreieich, Germany) with 0.05%
286 trifluoroacetic acid (4 min, 10 µL/min) and separated on a C18 reversed phase column
287 (SilicaTip™ emitter, 75 µm i.d., 8 µm tip, New Objective, Inc, Littleton, USA, manually packed
288 23 cm with ReproSil-Pur ODS-3, 3 µm particles, Dr. A. Maisch HPLC GmbH, Ammerbuch-
289 Entringen, Germany; flow rate: 300 nL/min). For sample injection and multi-step gradient
290 formation (eluent "A": 0.5% acetic acid in water; eluent "B": 0.5% acetic acid in 80%

291 acetonitrile / 20% water; gradient length / acquisition time: 100 min or 175 min) an UltiMate
292 3000 RSLCnano system (Thermo Fisher Scientific GmbH, Dreieich, Germany) was used.
293 Eluting peptides were electrosprayed at 2.3 kV via a Nanospray Flex ion source into a Q
294 Exactive HF-X hybrid quadrupole-orbitrap mass spectrometer (both Thermo Fisher Scientific
295 GmbH, Dreieich, Germany) and analyzed by data-dependent acquisition with HCD (higher
296 energy collisional dissociation) fragmentation of doubly, triply and quadruply charged ions
297 (loop count and dynamic exclusion dependent on the gradient length). Peak lists were generated
298 with ProteoWizard msConvert (http://proteowizard.sourceforge.net/; version 3.0.11098), linear
299 shift mass recalibrated (after a preliminary database search) using software developed in-house
300 and searched against a database containing the SARS-CoV-2 UniProtKB reference proteome
301 (proteome ID: UP000464024), all human UniProtKB/Swiss-Prot entries, and optionally (to
302 reduce the number of incorrectly assigned matches) selected bacterial proteins (finally the
303 Pseudomonas fluorescens (strain SBW25) reference proteome; proteome ID: UP000002332)
304 with Mascot 2.6.2 (Matrix Science Ltd, London, UK; peptide mass tolerance: ± 5 ppm;
305 fragment mass tolerance: ± 20 mmu; one missed trypsin cleavage and common variable
306 modifications allowed).
307
308 **Neutralization assay**
309 Serum neutralization capacity was analyzed as previously described (46). Briefly, VeroE6 cells
310 were seeded in 12-well plates at a density of $2.8x10^5$ cells/well 24 h prior to infection. Serum
311 samples were diluted at ratios of 1:16, 1:32 and 1:64 in 50 µL PBS total volume. Negative
312 controls (PBS without serum) were included for each serum. Diluted sera and negative controls
313 were subsequently mixed with 90 plaque forming units (PFU) of authentic SARS-CoV-2 (B.1)
314 in 50 µl PBS (1600 PFU/mL) resulting in final sera dilution ratios of 1:32, 1:64, and 1:128.
315 Following incubation at RT for 1 h, 400 µL PBS was added to each sample and the mixture
316 was subsequently used to infect VeroE6 cells. After 1.5 h of incubation at RT, inoculum was
317 removed and the cells were overlaid with 0.6% Oxoid-agar in DMEM, 20 mM HEPES (pH
318 7.4), 0.1% $NaHCO_3$, 1% BSA and 0.01% DEAE-Dextran. Cells were fixed 48 h post-infection
319 (4% formaldehyde for 30 minutes). Upon removal of the agar overlay, plaque neutralization
320 was visualized using 1% crystal violet. PFU were counted manually. Plaques counted for
321 serum-treated wells were compared to the average number of plaques in the untreated negative
322 controls, which were set to 100%.
323
324 **Ethics**
325 The protocol of this study conforms to the ethical guidelines of the 1975 Declaration of Helsinki
326 and was approved by the institutional ethical committee of the University of Freiburg (EK
327 153/20). Written informed consent was obtained from participants and the study was conducted
328 according to federal guidelines, local ethics committee regulations (Albert-Ludwigs-
329 Universität, Freiburg, Germany: No. F-2020-09-03-160428 and no. 322/20; No 507/16 and
330 624/14 for the SLE patients).
331
332 **Statistical analyses**
333 Statistical analyses were performed using linear statistical models. i.e. the two-group
334 comparisons were made based on the t-statistic of the estimated effects. Differences over more
335 than two groups were tested by Analysis of Variance (ANOVA) and multiple testing for
336 subsequent two-group comparisons was then considered by performing Games-Howell post-
337 hoc tests. For the time course data, patient differences were treated as random effects in a linear
338 mixed effects model with time and clinical course (severe vs. critical) as fixed main and
339 interaction effects. All analyses were performed at the log_2 scale. Assumptions about variance
340 heterogeneity and normal distribution were checked by visual inspection of diagnostic plots.
341

342 **Data and materials availability**
343 All data associated with this study are present in the paper or Supplementary Materials.
344
345
346 **Results**
347
348 **Patients and clinical information.**
349 We retrospectively analyzed serial serum samples collected for routine diagnostic testing from
350 41 patients hospitalized at our tertiary care center between March and June 2020 with SARS-
351 CoV-2 infection confirmed by real-time PCR. Based on the clinical course, we categorized
352 patients as either severely diseased (hospitalized with COVID-19 related pneumonia) versus
353 critically diseased (COVID-19 related pneumonia and eventually in need of invasive
354 mechanical ventilation). In total, 27 patients with critical and 14 with severe courses of disease
355 were grouped into separate cohorts (Table 1). Most patients were older than 60 years with an
356 overall mean age of 68 years (63 years and 76 years in the critically and severely diseased
357 patients respectively). The majority of patients in both groups had comorbidities of different
358 origin with cardiovascular diseases including hypertension representing the most frequent
359 pathology (35/41, 85%). Similar to previous reports, high Interleukin 6 (IL-6) and C-reactive
360 protein (CRP) levels were associated with severity of disease (Ø IL-6: 1452.1 pg/ml in the
361 critical group vs 46.1 pg/ml in the severe group and Ø CRP: 162.2 mg/l vs 65.3 mg/l, Ø13-25
362 days post symptom onset respectively). Similarly, procalcitonin, a biomarker of microbial
363 coinfection, was significantly higher in critically diseased patients (Ø value 9.9 ng/ml vs 0.17
364 ng/ml). Bacterial superinfection represented a further complication in 39% of the patients and
365 was only slightly more frequent in patients with critical disease (11/27, 41% vs 5/14, 33%).
366 More than half of the patients (59%) were treated with hydroxychloroquine/Lopinavir and
367 Ritonavir (Kaletra®), (18/27, 67% in the critical group vs 6/14, 43% in the severe group).
368 Notably, at the time of serum acquisition, only one patient received steroid treatment, which
369 was given due to underlying chronic obstructive pulmonary disease. Finally, mortality rate was
370 37% (10/27) in critically and 7% (1/14) in severely diseased patients.
371
372

Table 1: Clinical characteristics of the hospitalized SARS-CoV-2 patients.
Patients were categorized as either severely (hospitalized, requiring O_2 supplementation, n=14) or critically diseased (hospitalized and in need of invasive mechanical ventilation, n=27). Diagnostic markers are depicted as mean and SD (in brackets) of all analyzed laboratory parameters obtained 13-25 days post symptom onset. Percentage [%] is indicated.

	All patients n: 41	**%**	**critical** n: 27	**%**	**severe** n: 14	**%**
Age [years]	Ø 68 (31-90)	-	Ø 63 (39-79)	-	Ø 76 (31-90)	-
Female	8	19.5	5	18.5	3	21.4
Male	33	80.5	22	81.5	11	78.6
Comorbidities						
Hypertension	21	51.2	12	44.4	9	64.3
Cardiovascular disease	14	34.1	5	18.5	9	64.3
Pulmonary disease	6	14.6	2	7.4	4	28.6
Chronic kidney disease	6	14.6	1	3.7	5	35.7
Diabetes	10	24.4	6	22.2	4	28.6
Malignancy	8	19.5	4	14.8	4	28.6
none	6	14.6	6	22.2	0	0
Diagnostic markers						
Interleukin-6 [pg/ml] Ø	1012.8	-	1452.1 (3774.6)	-	46.1 (26.8)	-
Procalcitonin [ng/ml] Ø	7	-	9.9 (21.9)	-	0.17 (0.11)	-
C- reactive protein [mg/l] Ø	128.1	-	162.2 (75.8)	-	65.3 (47.1)	-
Complications						
Bacterial superinfection	16	39	11	40.7	5	35.7
Treatment						
Hydroxychloroquine, Ritonavir+ Lopinavir (Kaletra®)	24	58.5	18	66.7	6	42.9
Fatal outcome						
Total	11	26.8	10	37	1	7.1

Kinetics of IgG antibody responses following symptom onset across severe and critical courses of disease.
It has been observed that elevated SARS-CoV-2 antibody titers are associated with disease severity (15) and speculated to play a role not only in the clearance but also in the pathogenesis of SARS-CoV-2 infection (47). We initially analyzed the levels and kinetics of SARS-CoV-2 specific IgG in serial serum samples from patients hospitalized with critical (n=27) or severe (n=14) illness, a setting we also used in the following experiments. A total of 125 (critically diseased) and 79 (severely diseased) serum samples, obtained from the aforementioned patients at different time points within 6-25 days following symptom onset were analyzed by commercially available S1- and N- specific ELISA-based assays. Assay specificity was confirmed analyzing healthy donor (HD) serum samples (n=30) as negative control (Figure 1-figure supplement 1 A, B). Most patients developed detectable SARS-CoV-2 specific IgG responses within 9-14 days after symptom onset. SARS-CoV-2 specific IgG gradually increased over time in both severely and critically diseased patients reaching a plateau at 18-20

396 days after symptom onset (Figure 1 A, B). Varying antibody response kinetics were observed
397 for each individual patient (Figure 1-figure supplement 2 A-D) with anti-N IgG titers rising
398 significantly earlier than anti-S1 IgG (12.5 days ± 3.3 days vs 10.6 ± 3.8; p= 0.0091). A trend
399 towards earlier seroconversion for anti-S1 IgG could be observed in critically diseased patients
400 (mean time of seroconversion 11.4 ± 3.0 days in critically diseased patients vs 12.9 ± 3.8 days
401 for severely diseased patients; p = 0.24), whereas time of seroconversion for anti-N IgG was
402 similar in both groups (10.1 ± 3.2 and 10.4 ± 4.2 days for critically and severely diseased
403 patients, respectively; p = 0.83). S1- and N-specific IgG levels at plateau did not significantly
404 differ between the two groups. No significant difference between deceased and discharged
405 patients was measured 13-25 days after symptom onset (Figure 1- figure supplement 1 C, D,
406 E). Next, we evaluated and compared the neutralizing capacity of SARS-CoV-2 antibodies in
407 either critically versus severely diseased patients in a plaque-reduction assay (Figure 1 C). All
408 patients mounted a robust neutralizing antibody response (91% ± 10.5 % neutralization at a
409 1:64 serum dilution), with peaking titers at 18-20 days following symptom onset. Of note, two
410 critically diseased patients developed a neutralizing response already at 6-8 days after symptom
411 onset. In summary, we observed only minor differences in cohort wide kinetics of S1- or N-
412 specific IgG levels between patients hospitalized with severe or critical clinical courses
413 indicating that antibody levels per se did not correlate with severity of disease in our study.
414

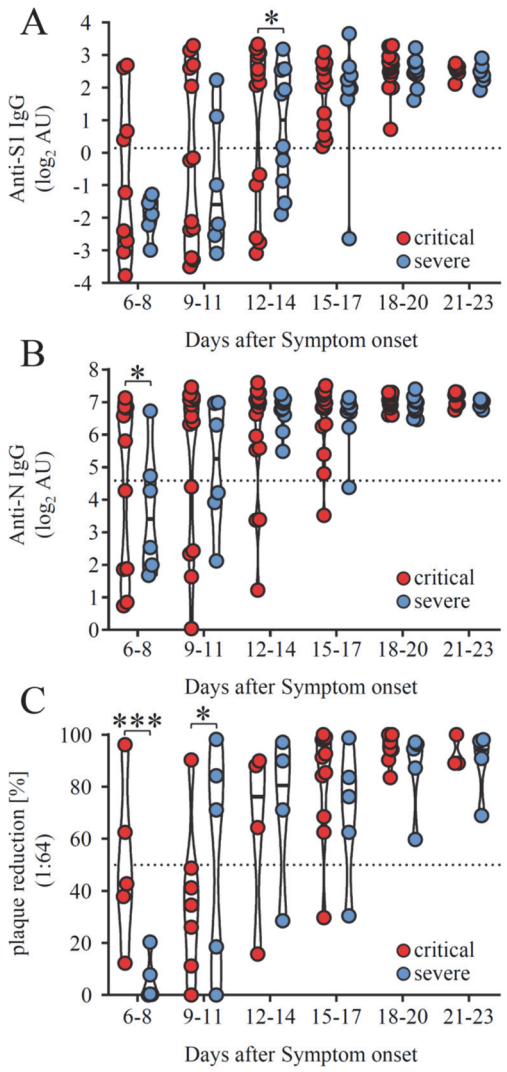

Figure 1. IgG responses against different SARS-CoV-2 proteins across severe and critical clinical course of disease.

IgG antibody levels were analyzed in longitudinal serum samples from hospitalized SARS-CoV-2 infected individuals. 27 patients were categorized as critically diseased when in need of invasive mechanical ventilation (red symbols) compared to 14 severely diseased patients who did not require invasive ventilation (blue symbols). (A) IgG response against SARS-CoV-2 S1 –protein and (B) SARS-CoV-2 N-protein as determined by commercial ELISA assays. Dotted lines represent cut-off values for commercial S1- and N- specific ELISA assays. Each dot represents the mean value obtained by the analysis of all samples which were available at the indicated time points following symptom onset. Solid black lines indicate the median. (C) Serum neutralization capacity against SARS-CoV-2 measured by a plaque reduction assay. Sera were considered neutralizing upon 50% plaque reduction (dotted line) at a 1:64 dilution. Solid black lines indicate the median. Significant differences were tested using a linear mixed effects model (***, $p<0.001$; *, $p<0.05$).

433 **Patients with severe COVID 19 show enhanced FcγRIII/CD16 activation by S-specific IgG**
434 **antibodies.**
435 FcγRIII (CD16) activation initiates multiple protective effector functions such as antibody-
436 dependent cellular cytotoxicity (ADCC) by natural killer (NK) cells as well as antibody-
437 dependent cytokine and chemokine secretion by NK cells and macrophages (18, 48). However,
438 excessive FcγR stimulation can have severe adverse effects such as elevated cytokine release
439 as observed in systemic autoimmune diseases or viral infections (18). Therefore, we
440 hypothesized that an exaggerated FcγR mediated activation triggered by SARS-CoV-2 specific
441 IgG might contribute to the exacerbation of COVID-19 in severely compared to critically
442 diseased patients. To address this, we analyzed the ability of SARS-CoV-2 specific antibodies
443 to activate CD16 (158V) using a previously validated cell-based reporter system (40-42, 49,
444 50) (Figure 2- figure supplement 1A). Considering the typically late time point of health
445 deterioration, we performed an analysis of CD16 activation triggered by SARS-CoV-2 specific
446 IgG with serum samples obtained 13-25 days following symptom onset (Figure 2). Sera were
447 analyzed at a 1:500 dilution to stay within the dynamic range of detection (Figure 2- figure
448 supplement 2). Depending on the availability of sample material 2-8 samples/patient/time-point
449 were included in this analysis. If available in sufficient quantity, sera were reanalyzed.
450 Reproducibility was tested using available serum surplus (Figure 2- figure supplement 3). Sera
451 from 28 patients with mild SARS-CoV-2 infection and 30 healthy blood donors were included
452 for reference. Semi-quantitative assessment of IgG titers using antigen-specific ELISA revealed
453 comparable levels between critically and severely diseased patient cohorts (Figure 2 A, B, C).
454 In contrast, S- ($p=0.0147$) and RBD-specific ($p=0.0120$) but not N-specific IgG-mediated CD16
455 activation was significantly increased in critically compared to severely diseased patients
456 (Figure 2 D-F). Furthermore, normalizing CD16 activation to antigen-specific IgG titers,
457 revealed significantly stronger CD16 activation by S- ($p=0.0033$) and N-specific ($p=0.006$) IgG
458 compared to mildly diseased patients (Figure 2 G-I). Intriguingly, we observed a heterogeneous
459 CD16 activation pattern characterized by either high or low CD16-activating sera irrespective
460 of the clinical manifestation (Figure 2 D-F). Overall, a significant positive correlation could be
461 determined between anti-SARS-CoV-2 antigen IgG titers and CD16 activation (Figure 2-figure
462 supplement 4). Our data document a sustained CD16 activation by SARS-CoV-2 specific
463 antibodies particularly in patients suffering from critical COVID-19 disease. Based on these
464 results we confirmed the notion that elevated FcγRIII/CD16 activation by S- and or RBD-
465 specific IgG might contribute to disease severity of COVID-19.
466

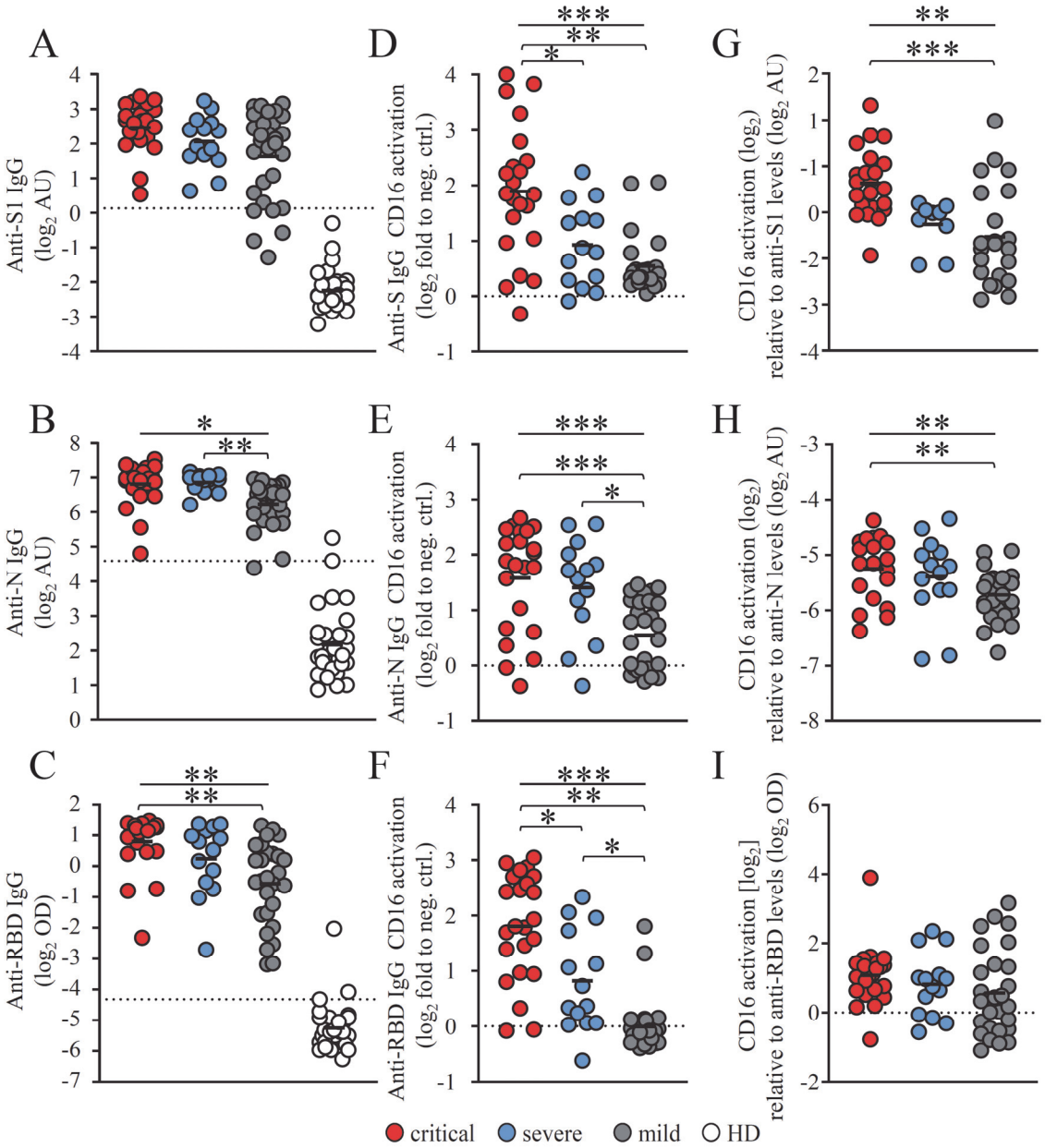

Figure 2. CD16 activation by SARS-CoV-2 - specific IgG is enhanced in critically diseased patients.

FcγRIII activation by SARS-CoV-2-specific IgG on BW5147 reporter cells in serum samples obtained 13-25 days following symptom onset from 23 critically (red symbols) and 14 severely (blue symbols) diseased patients. Between 2 to 8 samples/patient were analyzed depending on the availability of sample material. Sera from 29 non-hospitalized patients with mild SARS-CoV-2 infection (grey symbols) and 30 healthy donors (open circles) served as reference. Each symbol represents the mean value of all available samples per patient. (A, B, C) ELISA levels for S1- N- and RBD-specific IgG. Dotted lines represent cut-off values for commercial S1-, N- and RBD - specific ELISA assays. Solid black lines indicate the mean. (D, E, F) FcγRIII activation by S-, N- and RBD-specific IgG expressed as $\log_2$ fold change relative to negative control. Solid black lines indicate the mean. (G, H, I) FcγRIII activation, expressed as $\log_2$ values relative to SARS-CoV-2-spcific IgG titers. Solid black lines indicate the mean. Significant differences over all three groups were tested by ANOVA and pairwise group comparison was made by Games-Howell post-hoc tests (***, $p<0.001$; **, $p<0.01$; *, $p<0.05$).

Enhanced Fcγ-afucosylation of S-specific IgG in critically and severely diseased patients results in increased FcγRIII/CD16 activation.

Based on the findings described above we speculated that differences in Fcγ mediated effector functions might contribute to disease severity of COVID-19. We compared CD16 high- versus CD16 low-activating patient sera regarding their SARS-CoV-2 specific IgG core fucosylation. Inspired by previous findings (51-53) we focused on determining IgG core fucosylation of S- and N- specific SARS-CoV2 IgG. To determine IgG core fucosylation we used a lectin-based ELISA preceded by antigen-specific antibody purification from immobilized SARS-CoV-2-antigen. Analysis of anti-S and anti-N IgG core fucosylation was performed on serum pools containing five sera of either critically or severely diseased patients obtained 13-25 days post symptom onset. Given the aforementioned heterogeneity in CD16-activation, we analyzed pools of 5 sera of either critically or severely diseased patients characterized by either high or low CD16-activation. To stay within the dynamic detection range, relative fucosylation was analyzed at a dilution of 1:4 (Figure 3). When analyzing serum pools from critically and severely diseased patients we determined a significantly lower level of core fucosylation among the high CD16 activators (Figure 3, plain-colored bars) compared to the low CD16 activators (Figure 3, shaded bars). This applied for both the S- and N-specific antibodies. These results are in line with previously published findings regarding the effect of Fcγ-afucosylation on FcγRIII/CD16 effector functions (51, 54) and recapitulate similar findings in the context of COVID-19 (52, 53). However, we did not observe significant differences between critically and severely diseased patients.

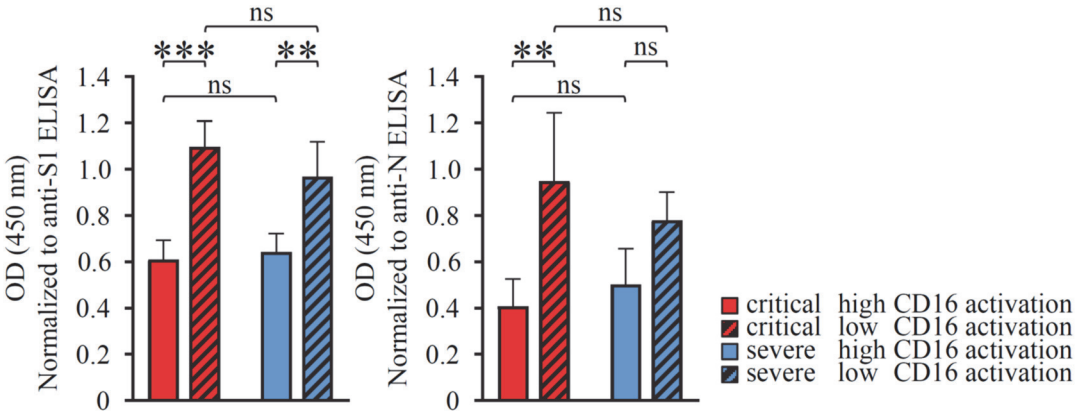

Figure 3. Anti SARS-CoV-2 IgG Fc core fucosylation in critical and severe COVID-19 cases.

IgG-Fc core fucosylation levels of SARS-CoV-2 –specific IgG in critically (red bars) and severely (blue bars) diseased COVID-19 patients. Analysis was carried out on a pool of 5 different sera. Measured OD values for fucosylation of the generated eluates were normalized to their respective IgG titers determined by antigen-specific S1 and N ELISA. A) S-IgG-Fc-fucosylation and B) N-IgG-Fc-fucosylation in critically and severely diseased patients characterized by either high (red) or low (patterned) CD16-activation levels in the FcγR activation reporter assay. The mean and standard deviation (SD) of at least three independent experiments is depicted. Statistical tests using a two-factorial linear model indicate three significant differences between the low and high categories (***, $p<0.001$; **, $p<0.01$; *, $p<0.05$; ns = not significant).

522 **COVID-19 disease severity correlates with an increase in FcγRIII/CD16-reactive soluble**
523 **IgG complexes.**
524 Next to afucosylation, it has been proposed that uncleared antigen-antibody immune complexes
525 (ICs) might be involved in the pathogenesis of severe COVID-19.(34-36, 38). However, the
526 actual presence of circulating, multimeric soluble ICs (sICs) in critically or severely diseased
527 patients has not been shown yet. As extensive FcγR activation by sICs might contribute to the
528 severe systemic inflammatory state occurring in some COVID-19 patients with prolonged
529 disease, we surmised that sICs might be a putative explanation for the marked differences in
530 IL-6, PCT and CRP levels between critically and severely diseased patients (Table 1). We thus
531 set out to characterize our patient cohort regarding the presence of sICs in serum samples taken
532 at various time points during disease and after hospitalization. To this end, we deployed a novel
533 cell-based reporter assay developed to quantify CD16 (158V) activation by IgG-containing
534 sICs, measuring their bioactivity (25, 44). This assay does not react to monomeric IgG or small
535 dimeric complexes in solution, but specifically identifies multimeric sICs and has been
536 successfully used to detect sICs in patients with systemic lupus erythematosus (SLE). In SLE,
537 sICs are major driver of inflammation (24). This assay showed, as judged by conventional
538 biomarkers, that sIC bioactivity correlates with SLE disease severity. Moreover, the assay is
539 sensitive to sICs size with larger complexes leading to stronger receptor activation compared
540 to small complexes (25). Analysis of serum samples, obtained 13-25 days after symptom onset,
541 revealed the presence of highly CD16-reactive sICs in SARS-CoV-2 infected patients
542 compared to healthy individuals (Figure 4A). Next, we compared sIC-mediated CD16
543 activation between COVID-19 patients of varying disease severity. While all COVID-19
544 patient groups tested positive for reactive sICs compared to healthy control (HD) sera, we found
545 that critically diseased patients show a striking increase in reactive sICs compared to patients
546 with severe or mild disease (Figure 4B). We then compared sIC bioactivity between sera from
547 critically diseased COVID-19 patients and sera from SLE patients with active disease (Figure
548 4C). We conclude that sICs formed in COVID-19 are comparable to sICs formed during active
549 SLE regarding their potential to drive inflammation. Only 6 out of 27 patients with critical
550 disease (22%) showed no sIC-mediated CD16 activation. As we did not detect highly reactive
551 sICs in the serum of 47 patients with acute respiratory distress syndrome (ARDS; mean age
552 57.5 years) in response to infections of different etiology including CMV reactivation,
553 HIV/AIDS, influenza or pulmonary TBC infection, we conclude that the formation of reactive
554 sICs is associated with severe SARS-CoV-2 disease (Figure 4-figure supplement 1).
555 Remarkably, longitudinal analysis of reactive sICs in the serum of critically or severely diseased
556 patients revealed high CD16 activation levels in 4 critically diseased patients already 6 to 8
557 days after symptom onset (Figure 4D). Of note, 2 of 4 patients with an early increase of
558 circulating reactive sIC eventually died. sIC-mediated CD16 activation persisted in 14 of 19
559 critically diseased patients at high levels until day 26 after symptom onset. sIC-mediated CD16
560 activation in severely diseased patients was slightly delayed compared to critically diseased
561 patients and was first detected in 4 patients 9-11 days after symptom onset (Figure 4D). Only 4
562 of 14 patients with severe disease showed detectable sIC-mediated CD16 activation. To verify
563 that sICs represent the CD16-reactive component in the serum of COVID-19 patients, we
564 analyzed serum-mediated CD16 activation before and after PEG8000-precipitation. This
565 treatment was previously shown to selectively precipitate large IgG complexes from solution
566 (25, 55). For this analysis, pools of 8 sera, showing either high (IC+) or no (IC-) CD16
567 activation, were compared. Sera from healthy donors (HD) served as a negative control.
568 Compatible with the hypothesis of serum-derived sICs driving CD16 activation, no activation
569 was observed following incubation with 3.5% PEG8000 (Figure 4-figure supplement 2 A). To
570 ensure that the treatment did not precipitate monomeric IgG, we tested the depleted sera for
571 remaining S1- and N-specific IgG. As depicted S1- and N- specific IgG could still be detected
572 at unchanged high levels in samples treated with 3.5% PEG8000 (Figure 4-figure supplement

573 2 B). When resolving sIC-mediated CD16 activation over the complete time of hospitalization
574 for select patients from which samples at different time points were available, we observed that
575 sIC reactivity predominantly precedes anti-S1 IgG in ELISA as well as CD16 activation by
576 SARS-CoV-2-specific IgG (Fig. 4-figure supplement 3, Fig. 4-figure supplement 5). This
577 implies that sIC formation does not depend on the presence of SARS-CoV-2 antigens.
578 Accordingly, we were not able to identify any SARS-CoV-2-derived antigens in PEG8000-
579 precipitated sICs using tandem mass spectrometry (data not shown). To further exclude the
580 formation of multimeric sICs formed from circulating S1 antigen, we also specifically targeted
581 S1 for precipitation from patient serum using biotinylated S1-specific monoclonal antibodies.
582 However and in line with our previous approach, S1-specific precipitation using streptavidin-
583 sepharose beads and subsequent mass spectrometry analysis for any SARS-CoV-2-specific
584 antigens in sICs remained without result (data not shown). Recently, the role of neutrophil
585 mediated intravascular NETosis was reported to play a critical role in thrombose formation and
586 subsequent organ damage observed in severe clinical forms of COVID-19 (56-58). Since this
587 process could mediate the formation of aggregated IgG as a form of sICs, we next tested
588 whether Benzonase® nuclease treatment of patient serum would dissolve reactive sICs. To this
589 end we tested sera from critically diseased patients or healthy individuals and compared CD16
590 reactivity before and after nuclease treatment (Figure 4-figure supplement 4). Nuclease activity
591 in diluted human serum was controlled using plasmid DNA for reference. This revealed that
592 nucleic acid was not involved in the formation of CD16-reactive sICs in critically diseased
593 patients. Finally, we tested pooled patient sera for autoantibodies against a panel of prototypical
594 autoantigens associated with autoimmune disease including anti-nuclear autoantibodies (ANA)
595 by indirect immunofluorescence, dsDNA autoantibodies by ELISA and autoantibodies against
596 the extractable nuclear antigens (nRNP/Sm, Sm, SS-A, Ro-52, SS-B, Scl-70, PM-Scl, Jo-1,
597 CENP B, PCNA, nucleosomes, histones, ribosomal P-protein, AMA-M2, DFS70) by dot blot
598 in case SARS-CoV-2 infection triggers autoantibody formation and possible sIC formation.
599 However, no significant autoantibody titers could be detected in any sera pool (data not shown).
600 Although we were not able to identify their origin, our data clearly indicates the presence of
601 circulating sICs in COVID-19 patients with an increase in CD16-reactive sICs corresponding
602 with severity of disease and reaching activation levels comparable to those observed in SLE
603 patients with active disease. Accordingly, we conclude that circulating sICs are a hitherto
604 unknown, yet contributing factor to COVID-19 disease severity and, regarding infectious
605 diseases, our findings represent an observation unique to severely diseased COVID-19 patients.
606

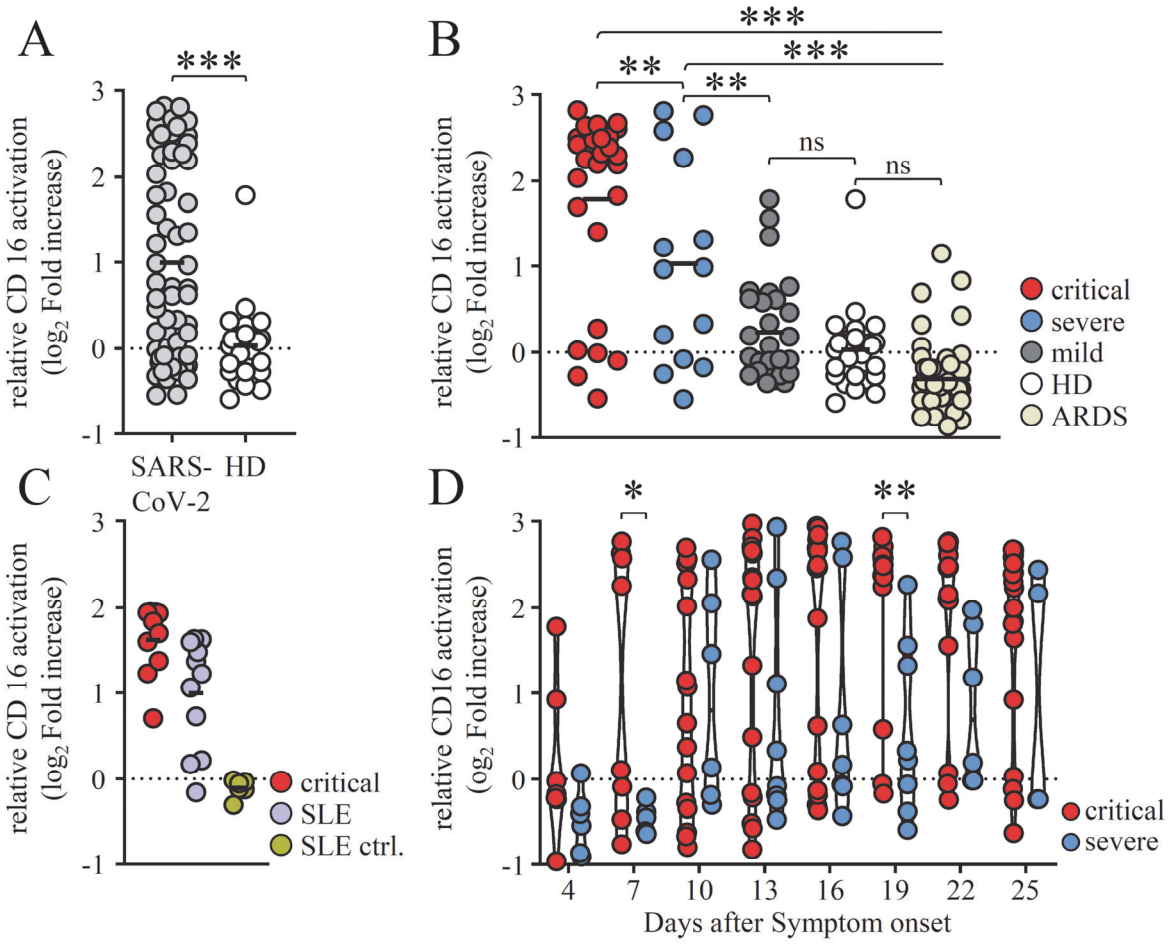

Figure 4. Severe COVID-19 disease coincides with high CD16 activation by sICs. Serial serum samples obtained 13-25 days after onset of symptoms were analyzed in a cell-based reporter assay which is sensitive to sIC amount and size (25, 44). FcγR activation is shown as $\log_2$ fold change relative to negative control. Each symbol represents the mean value obtained by the analysis of all samples available in the indicated time range for each individual patient. A) Analysis of CD16 activation by sICs in SARS-CoV-2-infected patients compared to healthy blood donors B) Levels of IC-mediated CD16 activation across severe, critical and mild clinical courses of COVID-19 disease, in healthy donors (HD) and in non-COVID-19 patients who developed acute respiratory distress syndrome (ARDS). Solid black lines indicate the mean. Two-group comparisons with the linear model indicate significant differences between critical cases and all other groups, as well as between severe cases and all other groups (***, $p<0.001$; **, $p<0.01$). No significant differences ($p>0.05$) have been found for the comparisons mild vs. healthy and for HD vs. ARDS. C) Select sera from critically diseased patients were compared to sera from SLE patients with active disease regarding CD16 activation. Sera from healthy donors served as SLE-negative control. Solid black lines indicate the mean. D) Kinetics of IC-mediated CD16 activation in critically and severely diseased patients. Days after symptom onset are depicted as a range (+/- 1 day). Solid black lines indicate the median. The mixed effects model indicates two time points with significant differences (**, $p<0.01$; *, $p<0.05$).

629 **Discussion**
630
631 We collected and analyzed data from 41 COVID-19 patients hospitalized at the University
632 Hospital Freiburg. Patients were categorized by severity of disease into severely (n=14) and
633 critically diseased patients (n=27). Both groups were of comparable average age and had a
634 similar male-to-female ratio. For comparison we also analyzed 28 mildly diseased and 30
635 healthy individuals. As key findings we identify *de novo* produced afucosylated SARS-CoV-2
636 IgG and the presence of soluble circulating immune complexes (sICs) activating FcγRIII/CD16
637 as potential risk factors closely associated COVID-19 severity.
638
639 **Circulating sICs contribute to COVID-19 disease severity.**
640 Using an adapted reporter cell activation assay optimized to detect sICs (25, 44) we provide
641 first evidence of circulating sICs in the serum of COVID-19 patients and experimentally
642 confirm previous hypotheses suggesting immune complexes as potential drivers of disease
643 progression in COVID-19 (34-36, 38). In fundamental contrast to opsonized antigens
644 decorating virus-infected cells in tissues, sICs become distributed systemically. Thus
645 constitutive activation of $CD16^+$ monocytes, granulocytes and NK cells could readily explain
646 systemic responses which potentiate local inflammation in virus-infected tissues intensifying
647 organ damage and dysfunction. Although the origin of the circulating immune complexes and
648 the nature of the bound antigens still remains elusive, we clearly show that the presence of IgG-
649 containing sICs during SARS-CoV-2 infection is directly responsible and sufficient for the
650 observed FcγRIII/CD16 activation by patient serum. Recent work has shown that viral antigens
651 can be detected in the serum of patients (59, 60). However, as we find sIC reactivity to
652 predominantly precede SARS-CoV-2-S specific IgG responses, we conclude that circulating S
653 or shed S1-antigens are not involved in sIC formation. Since sICs are commonly associated
654 with immunopathology in autoimmunity (23, 24, 61) and several studies have described that a
655 variety of specific auto-antibodies can be detected in certain critically ill COVID-19 patients
656 (62-64), we could not identify a distinct culprit antigen linked to sIC formation when searching
657 for prototypical autoantibodies. However, as sIC formation is strongly reminiscent to SLE and
658 sICs initiate a common terminal pathway of inflammation we classified patients as sIC-prone
659 or non-sIC-prone (graphical abstract). Of note, besides sIC formation a range of additional
660 phenotypical abnormalities shared between B cell populations in autoimmune disorders
661 exemplified by active SLE and severe COVID-19 have been observed. This includes the
662 pronounced engagement of extrafollicular B cell responses, associated with the activation of
663 effector B cells lacking naïve (IgD) and memory markers (CD27) as well as class-switched
664 antibody secreting cells (62).
665 We suggest a hidden predisposition in sIC-prone patients resulting in a strong early
666 inflammatory response to SARS-CoV-2 infection possibly being a trigger for further sIC
667 formation and the generation of afucosylated SARS-CoV-2 IgG. Very recent work reports that
668 an acute SARS-CoV-2 infection triggers the *de novo* IgG production against multiple
669 autoantigens. In this study, 60-80% of all hospitalized COVID-19 patients exhibited anti-
670 cytokine IgG (ACA) (65). The authors show that ACA levels and specificity change over time
671 during hospitalization, suggesting ACA induction in response to viral infection and
672 inflammation. Further, it has been shown that pre-existing neutralizing anti-type I interferon
673 antibodies, which can be found in about 10% of patients with severe COVID-19 pneumonia,
674 are related to the highest risk of developing life-threatening COVID-19 disease (66). Therefore,
675 the *de novo* induction of anti-cytokine auto-antibodies in a large proportion of hospitalized
676 COVID-19 patients as described by Chang et al. (65), might indeed represent a source of
677 circulating sICs in COVID-19. In such a scenario, immune responses are deviated first by an
678 immunodepletion of critical cytokines and second through the formation of pathological sICs
679 which trigger immunological damage. We show that critically diseased patients exhibit

significantly higher levels of reactive sICs compared to less severely diseased patients. Notably, CD16 activation levels in patients with critical disease were comparable to those measured in SLE patients, where circulating sICs have long been shown to crucially contribute to tissue damage and disease manifestations (67, 68). In addition, sIC responses can be found significantly earlier in critically diseased patients, which was associated with a fatal disease outcome. We also find that patients show a wide range of sIC reactivity. According to the Heidelberger-Kendall precipitation curve (69), sIC size is critically dependent on the antigen:antibody stoichiometry. As the used FcγR activation assay is highly sensitive to sIC size (25), it is likely that this also plays a role when detecting this bioactivity in COVID-19 patient serum. Therefore, we propose that in addition to the presence of sICs, the size of sICs plays a role in CD16 driven COVID-19 immunopathology. Based on these findings, together with the higher levels of afucosylation, we conclude that CD16 activation in COVID-19 disease is governed by sIC formation and IgG glycan profiles (Figure 5). It can be hypothesized that the formation of sICs in predisposed patients initiates a vicious circle of FcγR-mediated inflammation leading to an increase of IgG afucosylation, followed by enhanced FcγR activation by SARS-CoV-2-specific IgG, further contributing to inflammation and, conceivably, to *de-novo* sIC formation. Indeed, there is evidence in this direction from a clinical perspective provided by a recent study that finds the administration of intravenous immunoglobulin (IVIg) to alleviate COVID-19 disease (70). Although no direct proof, this heavily implies that the saturation of FcγRs mitigates immunopathology as previously reported for autoimmune diseases (71). Therefore, our findings provide an explanation for the sustained immunopathology following SARS-CoV-2 infection observed in some patients as well as for the efficacy of IVIg treatment in severe to critical COVID-19 disease. Finally, when we analyzed sera from COVID-19 patients obtained during the following waves of the pandemic, we again found comparable levels of reactive sICs in the serum of critically diseased patients (data not shown) implying that sIC formation in COVID-19 is conserved across different SARS-CoV-2 strains. It will be important to investigate whether such sICs may persist in reconvalescent patients and might be an explanation for immune alterations including auto-antibodies observed in patients with persistent long COVID-19 symptoms (72).

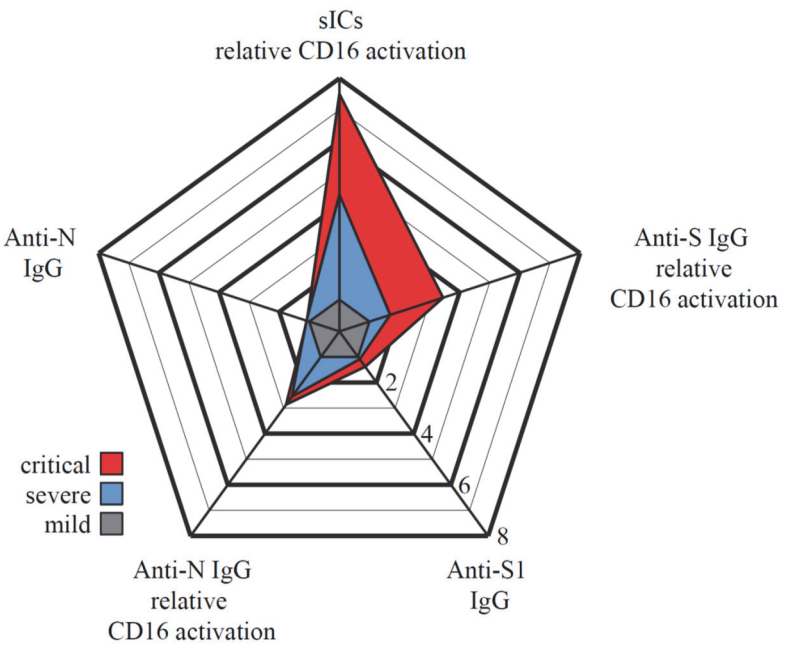

Figure 5. Summary of antibody features from SARS-CoV-2-infected patients with critical and severe disease.

Relative multivariate antibody features illustrated as radar chart in critically (red) or severely (blue) diseased COVID-19 patients normalized to the corresponding features of patients with mild infection (grey). Each spoke represents one of the following variables: ELISA (S1-IgG, N-IgG,) and CD16 activation (S-IgG, N-IgG, multimeric sICs). Arithmetic mean values of $\log_2$ values were calculated for each group (days 13-25 post symptom onset) respectively. The fold change compared to mildly diseased patients is shown.

Acknowledgements
We thank Sophia Ruben and Torsten Schulz from InVivo Bio Tech Services for preparing SARS-CoV-2 (S)- and RBD- coated plates and preparing the SARS-CoV-2 IgG ELISA Reagent Set. We thank Hans-Martin Jäck for providing TRES-1-224.2.19 and TRES-II-480 monoclonal antibodies and Quinnlan David for critically reading the manuscript. We also thank Andreas Schlosser for validation of our Mass Spectrometry data.

Author contribution
Conceived and designed the experiments: J.A., A.M-P., S.G., P.K., A.L, V.F., M.S., H.H.
Performed the experiments: J.A., N.G., U.S., S.G., K. C., W.B.
Analyzed the data: J.A., S.G., P.K., V.F., K.C., A.M-P., W.B., C.K.
Contributed/reagent/sample material: A.B.G., D.H., T.W., NG.M., RE.V.
Writing and original draft preparation: J.A., S.G., P.K., V.F.
Review and editing: H.H., M.S., K.C.
Conceptualization: V.F., H.H.

References

1. Zhu N, Zhang D, Wang W, Li X, Yang B, Song J, et al. A Novel Coronavirus from Patients with Pneumonia in China, 2019. N Engl J Med. 2020;382(8):727-33.
2. Dong E, Du H, Gardner L. An interactive web-based dashboard to track COVID-19 in real time. Lancet Infect Dis. 2020;20(5):533-4.
3. Chen G, Wu D, Guo W, Cao Y, Huang D, Wang H, et al. Clinical and immunological features of severe and moderate coronavirus disease 2019. J Clin Invest. 2020;130(5):2620-9.
4. Petrilli CM, Jones SA, Yang J, Rajagopalan H, O'Donnell L, Chernyak Y, et al. Factors associated with hospital admission and critical illness among 5279 people with coronavirus disease 2019 in New York City: prospective cohort study. BMJ. 2020;369:m1966.
5. Huang C, Wang Y, Li X, Ren L, Zhao J, Hu Y, et al. Clinical features of patients infected with 2019 novel coronavirus in Wuhan, China. Lancet. 2020;395(10223):497-506.
6. Wang F, Hou H, Luo Y, Tang G, Wu S, Huang M, et al. The laboratory tests and host immunity of COVID-19 patients with different severity of illness. JCI Insight. 2020;5(10).
7. Felsenstein S, Herbert JA, McNamara PS, Hedrich CM. COVID-19: Immunology and treatment options. Clin Immunol. 2020;215:108448.
8. Wu C, Chen X, Cai Y, Xia J, Zhou X, Xu S, et al. Risk Factors Associated With Acute Respiratory Distress Syndrome and Death in Patients With Coronavirus Disease 2019 Pneumonia in Wuhan, China. JAMA Intern Med. 2020;180(7):934-43.
9. Magleby R, Westblade LF, Trzebucki A, Simon MS, Rajan M, Park J, et al. Impact of SARS-CoV-2 Viral Load on Risk of Intubation and Mortality Among Hospitalized Patients with Coronavirus Disease 2019. Clin Infect Dis. 2020.
10. Ruan Q, Yang K, Wang W, Jiang L, Song J. Correction to: Clinical predictors of mortality due to COVID-19 based on an analysis of data of 150 patients from Wuhan, China. Intensive Care Med. 2020;46(6):1294-7.
11. Zhou F, Yu T, Du R, Fan G, Liu Y, Liu Z, et al. Clinical course and risk factors for mortality of adult inpatients with COVID-19 in Wuhan, China: a retrospective cohort study. Lancet. 2020;395(10229):1054-62.
12. Yang X, Yu Y, Xu J, Shu H, Xia J, Liu H, et al. Clinical course and outcomes of critically ill patients with SARS-CoV-2 pneumonia in Wuhan, China: a single-centered, retrospective, observational study. Lancet Respir Med. 2020;8(5):475-81.
13. Richardson S, Hirsch JS, Narasimhan M, Crawford JM, McGinn T, Davidson KW, et al. Presenting Characteristics, Comorbidities, and Outcomes Among 5700 Patients Hospitalized With COVID-19 in the New York City Area. JAMA. 2020;323(20):2052-9.
14. Zhou Y, Fu B, Zheng X, Wang D, Zhao C, Qi Y, et al. Pathogenic T-cells and inflammatory monocytes incite inflammatory storms in severe COVID-19 patients. National Science Review. 2020;7(6):998-1002.
15. Long QX, Liu BZ, Deng HJ, Wu GC, Deng K, Chen YK, et al. Antibody responses to SARS-CoV-2 in patients with COVID-19. Nat Med. 2020;26(6):845-8.
16. Diao B, Wang C, Tan Y, Chen X, Liu Y, Ning L, et al. Reduction and Functional Exhaustion of T Cells in Patients With Coronavirus Disease 2019 (COVID-19). Front Immunol. 2020;11:827.
17. Zhang JM, An J. Cytokines, inflammation, and pain. Int Anesthesiol Clin. 2007;45(2):27-37.
18. Vogelpoel LT, Baeten DL, de Jong EC, den Dunnen J. Control of cytokine production by human fc gamma receptors: implications for pathogen defense and autoimmunity. Front Immunol. 2015;6:79.
19. Ritz J, Schmidt RE, Michon J, Hercend T, Schlossman SF. Characterization of functional surface structures on human natural killer cells. Adv Immunol. 1988;42:181-211.
20. Werfel T, Uciechowski P, Tetteroo PA, Kurrle R, Deicher H, Schmidt RE. Activation of cloned human natural killer cells via Fc gamma RIII. J Immunol. 1989;142(4):1102-6.
21. Bruhns P, Jonsson F. Mouse and human FcR effector functions. Immunol Rev. 2015;268(1):25-51.

22. Zubler RH, Nydegger U, Perrin LH, Fehr K, McCormick J, Lambert PH, et al. Circulating and intra-articular immune complexes in patients with rheumatoid arthritis. Correlation of 125I-Clq binding activity with clinical and biological features of the disease. J Clin Invest. 1976;57(5):1308-19.
23. Levinsky RJ. Role of circulating soluble immune complexes in disease. Arch Dis Child. 1978;53(2):96-9.
24. Levinsky RJ, Cameron JS, Soothill JF. Serum immune complexes and disease activity in lupus nephritis. Lancet. 1977;1(8011):564-7.
25. Chen H, Maul-Pavicic A, Holzer M, Salzer U, Chevalier N, Voll RE, et al. FcγR responses to soluble immune complexes are governed by solubility and size. bioRxiv. 2021:2020.11.11.378232.
26. Wang TT, Ravetch JV. Immune complexes: not just an innocent bystander in chronic viral infection. Immunity. 2015;42(2):213-5.
27. Carreno LJ, Pacheco R, Gutierrez MA, Jacobelli S, Kalergis AM. Disease activity in systemic lupus erythematosus is associated with an altered expression of low-affinity Fc gamma receptors and costimulatory molecules on dendritic cells. Immunology. 2009;128(3):334-41.
28. Faik I, van Tong H, Lell B, Meyer CG, Kremsner PG, Velavan TP. Pyruvate Kinase and Fcgamma Receptor Gene Copy Numbers Associated With Malaria Phenotypes. J Infect Dis. 2017;216(2):276-82.
29. Xu Z, Shi L, Wang Y, Zhang J, Huang L, Zhang C, et al. Pathological findings of COVID-19 associated with acute respiratory distress syndrome. Lancet Respir Med. 2020;8(4):420-2.
30. Channappanavar R, Perlman S. Pathogenic human coronavirus infections: causes and consequences of cytokine storm and immunopathology. Seminars in Immunopathology. 2017;39(5):529-39.
31. Smits SL, de Lang A, van den Brand JM, Leijten LM, van IWF, Eijkemans MJ, et al. Exacerbated innate host response to SARS-CoV in aged non-human primates. PLoS Pathog. 2010;6(2):e1000756.
32. Rockx B, Baas T, Zornetzer GA, Haagmans B, Sheahan T, Frieman M, et al. Early upregulation of acute respiratory distress syndrome-associated cytokines promotes lethal disease in an aged-mouse model of severe acute respiratory syndrome coronavirus infection. J Virol. 2009;83(14):7062-74.
33. Hoepel W, Chen HJ, Geyer CE, Allahverdiyeva S, Manz XD, de Taeye SW, et al. High titers and low fucosylation of early human anti-SARS-CoV-2 IgG promote inflammation by alveolar macrophages. Sci Transl Med. 2021;13(596).
34. Roncati L, Ligabue G, Fabbiani L, Malagoli C, Gallo G, Lusenti B, et al. Type 3 hypersensitivity in COVID-19 vasculitis. Clinical Immunology. 2020;217.
35. Roe K. High COVID-19 virus replication rates, the creation of antigen-antibody immune complexes and indirect haemagglutination resulting in thrombosis. Transbound Emerg Dis. 2020;67(4):1418-21.
36. Zhang Y, Xiao M, Zhang S, Xia P, Cao W, Jiang W, et al. Coagulopathy and Antiphospholipid Antibodies in Patients with Covid-19. N Engl J Med. 2020;382(17):e38.
37. Carvelli J, Demaria O, Vely F, Batista L, Chouaki Benmansour N, Fares J, et al. Association of COVID-19 inflammation with activation of the C5a-C5aR1 axis. Nature. 2020;588(7836):146-50.
38. Manzo G. COVID-19 as an Immune Complex Hypersensitivity in Antigen Excess Conditions: Theoretical Pathogenetic Process and Suggestions for Potential Therapeutic Interventions. Front Immunol. 2020;11:566000.
39. Mazzitelli I, Bleichmar L, Luduena MG, Pisarevsky A, Labato M, Chiaradia V, et al. Immunoglobulin G Immune Complexes May Contribute to Neutrophil Activation in the Course of Severe Coronavirus Disease 2019. J Infect Dis. 2021;224(4):575-85.
40. Kolb P, Sijmons S, McArdle MR, Taher H, Womack J, Hughes C, et al. Identification and Functional Characterization of a Novel Fc Gamma-Binding Glycoprotein in Rhesus Cytomegalovirus. J Virol. 2019;93(4).
41. Kolb P, Hoffmann K, Sievert A, Reinhard H, Merce-Maldonado E, Le-Trilling VTK, et al. Human Cytomegalovirus antagonizes activation of Fcgamma receptors by distinct and synergizing modes of IgG manipulation. Elife. 2021;10.

842 42. Corrales-Aguilar E, Trilling M, Reinhard H, Merce-Maldonado E, Widera M, Schaal H, et al. A
843 novel assay for detecting virus-specific antibodies triggering activation of Fe gamma receptors. J
844 Immunol Methods. 2013;387(1-2):21-35.
845 43. Amanat F, Stadlbauer D, Strohmeier S, Nguyen THO, Chromikova V, McMahon M, et al. A
846 serological assay to detect SARS-CoV-2 seroconversion in humans. Nat Med. 2020;26(7):1033-6.
847 44. Zhao S, Grieshaber-Bouyer R, Rao DA, Kolb P, Chen H, Andreeva I, et al. JAK inhibition prevents
848 the induction of pro-inflammatory HLA-DR(+) CD90(+) RA synovial fibroblasts by IFN. Arthritis
849 Rheumatol. 2021.
850 45. Pandey A, Andersen JS, Mann M. Use of mass spectrometry to study signaling pathways. Sci
851 STKE. 2000;2000(37):pl1.
852 46. Tönshoff B, Müller B, Elling R, Renk H, Meissner P, Hengel H, et al. Prevalence of SARS-CoV-2
853 Infection in Children and Their Parents in Southwest Germany. JAMA Pediatrics. 2021;175(6):586-93.
854 47. Zohar T, Alter G. Dissecting antibody-mediated protection against SARS-CoV-2. Nat Rev
855 Immunol. 2020;20(7):392-4.
856 48. Lu LL, Suscovich TJ, Fortune SM, Alter G. Beyond binding: antibody effector functions in
857 infectious diseases. Nat Rev Immunol. 2018;18(1):46-61.
858 49. Perez-Portilla A, Moraru M, Blazquez-Moreno A, Kolb P, Bravo Garcia-Morato M, Ranganath T,
859 et al. Identification of the first cases of complete CD16A deficiency: Association with persistent EBV
860 infection. J Allergy Clin Immunol. 2020;145(4):1288-92.
861 50. Corrales-Aguilar E, Trilling M, Reinhard H, Falcone V, Zimmermann A, Adams O, et al. Highly
862 individual patterns of virus-immune IgG effector responses in humans. Medical microbiology and
863 immunology. 2016;205(5):409-24.
864 51. Chakraborty S, Gonzalez J, Edwards K, Mallajosyula V, Buzzanco AS, Sherwood R, et al.
865 Proinflammatory IgG Fc structures in patients with severe COVID-19. Nat Immunol. 2021;22(1):67-73.
866 52. High titers and low fucosylation of early human anti-SARS-CoV-2 IgG promote inflammation by
867 alveolar macrophages. Sci Transl Med. 2021.
868 53. Larsen MD, de Graaf EL, Sonneveld ME, Plomp HR, Nouta J, Hoepel W, et al. Afucosylated IgG
869 characterizes enveloped viral responses and correlates with COVID-19 severity. Science.
870 2021;371(6532).
871 54. Li T, DiLillo DJ, Bournazos S, Giddens JP, Ravetch JV, Wang LX. Modulating IgG effector function
872 by Fc glycan engineering. Proceedings of the National Academy of Sciences of the United States of
873 America. 2017;114(13):3485-90.
874 55. Creighton WD, Lambert PH, Miescher PA. Detection of antibodies and soluble antigen-
875 antibody complexes by precipitation with polyethylene glycol. J Immunol. 1973;111(4):1219-27.
876 56. Veras FP, Pontelli MC, Silva CM, Toller-Kawahisa JE, de Lima M, Nascimento DC, et al. SARS-
877 CoV-2-triggered neutrophil extracellular traps mediate COVID-19 pathology. J Exp Med. 2020;217(12).
878 57. Zuo Y, Yalavarthi S, Shi H, Gockman K, Zuo M, Madison JA, et al. Neutrophil extracellular traps
879 in COVID-19. JCI Insight. 2020;5(11).
880 58. Bonaventura A, Vecchie A, Dagna L, Martinod K, Dixon DL, Van Tassell BW, et al. Endothelial
881 dysfunction and immunothrombosis as key pathogenic mechanisms in COVID-19. Nat Rev Immunol.
882 2021;21(5):319-29.
883 59. Ogata AF, Maley AM, Wu C, Gilboa T, Norman M, Lazarovits R, et al. Ultra-Sensitive Serial
884 Profiling of SARS-CoV-2 Antigens and Antibodies in Plasma to Understand Disease Progression in
885 COVID-19 Patients with Severe Disease. Clin Chem. 2020;66(12):1562-72.
886 60. Shan D, Johnson JM, Fernandes SC, Suib H, Hwang S, Wuelfing D, et al. N-protein presents early
887 in blood, dried blood and saliva during asymptomatic and symptomatic SARS-CoV-2 infection. Nat
888 Commun. 2021;12(1):1931.
889 61. Thanadetsuntorn C, Ngamjanyaporn P, Setthaudom C, Hodge K, Saengpiya N, Pisitkun P. The
890 model of circulating immune complexes and interleukin-6 improves the prediction of disease activity
891 in systemic lupus erythematosus. Sci Rep. 2018;8(1):2620.

892 62. Woodruff MC, Ramonell RP, Nguyen DC, Cashman KS, Saini AS, Haddad NS, et al. Extrafollicular
893 B cell responses correlate with neutralizing antibodies and morbidity in COVID-19. Nat Immunol.
894 2020;21(12):1506-16.
895 63. Wang EY, Mao T, Klein J, Dai Y, Huck JD, Jaycox JR, et al. Diverse functional autoantibodies in
896 patients with COVID-19. Nature. 2021.
897 64. Zuo Y, Estes SK, Ali RA, Gandhi AA, Yalavarthi S, Shi H, et al. Prothrombotic autoantibodies in
898 serum from patients hospitalized with COVID-19. Sci Transl Med. 2020;12(570).
899 65. Chang SE, Feng A, Meng W, Apostolidis SA, Mack E, Artandi M, et al. New-Onset IgG
900 Autoantibodies in Hospitalized Patients with COVID-19. medRxiv. 2021.
901 66. Bastard P, Rosen LB, Zhang Q, Michailidis E, Hoffmann HH, Zhang Y, et al. Autoantibodies
902 against type I IFNs in patients with life-threatening COVID-19. Science. 2020;370(6515).
903 67. Nydegger UE, Davis JSt. Soluble immune complexes in human disease. CRC Crit Rev Clin Lab
904 Sci. 1980;12(2):123-70.
905 68. Koffler D, Agnello V, Thoburn R, Kunkel HG. Systemic lupus erythematosus: prototype of
906 immune complex nephritis in man. J Exp Med. 1971;134(3):169-79.
907 69. Heidelberger M, Kendall FE. A Quantitative Study of the Precipitin Reaction between Type Iii
908 Pneumococcus Polysaccharide and Purified Homologous Antibody. J Exp Med. 1929;50(6):809-23.
909 70. Gharebaghi N, Nejadrahim R, Mousavi SJ, Sadat-Ebrahimi SR, Hajizadeh R. The use of
910 intravenous immunoglobulin gamma for the treatment of severe coronavirus disease 2019: a
911 randomized placebo-controlled double-blind clinical trial. BMC Infect Dis. 2020;20(1):786.
912 71. Shock A, Humphreys D, Nimmerjahn F. Dissecting the mechanism of action of intravenous
913 immunoglobulin in human autoimmune disease: Lessons from therapeutic modalities targeting
914 Fcgamma receptors. J Allergy Clin Immunol. 2020;146(3):492-500.
915 72. Wallukat G, Hohberger B, Wenzel K, Furst J, Schulze-Rothe S, Wallukat A, et al. Functional
916 autoantibodies against G-protein coupled receptors in patients with persistent Long-COVID-19
917 symptoms. J Transl Autoimmun. 2021;4:100100.
918
919
920
921
922
923
924
925
926
927
928
929
930
931
932
933
934
935
936
937

938 **Supplementary Figures**
939
940
941 **Figure 1-figure supplement 1.**
942

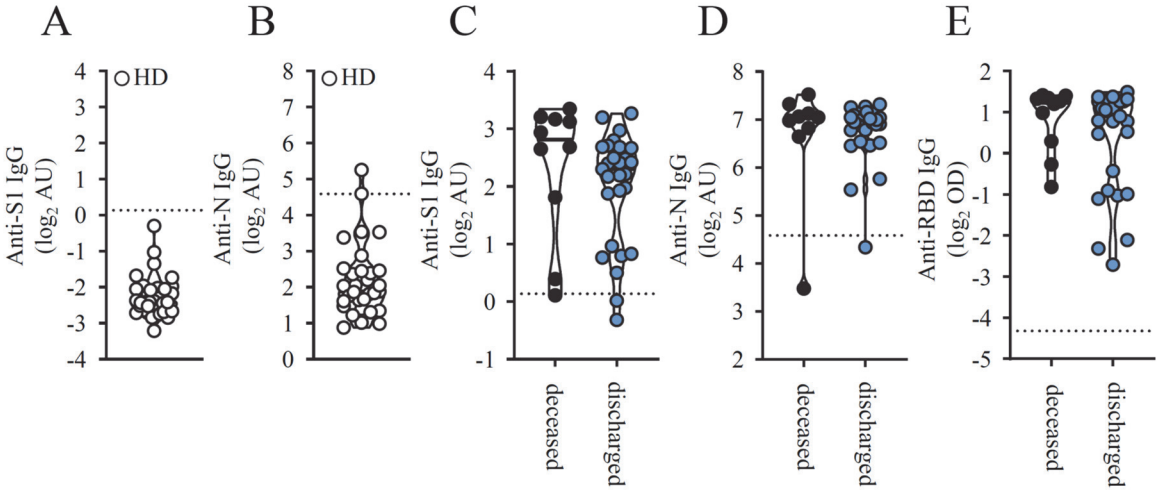

943
944
945 **SARS-CoV-2 specific IgG levels in seronegative patients and according to disease**
946 **outcome.**
947 A) S1- and B) N-specific IgG levels in 30 healthy donors. Solid black lines indicate the median.
948 C) Cumulative S1-, D) N- and E) RBD-specific IgG levels measured 13-25 days after symptom
949 onset in deceased (black symbols) and not deceased COVID-19 patients (blue symbols). Each
950 symbol represents the mean value obtained by the analysis of all samples available in the
951 indicated time range for each individual patient. Solid black lines indicate the median.
952
953

954 **Figure 1-figure supplement 2.**
955

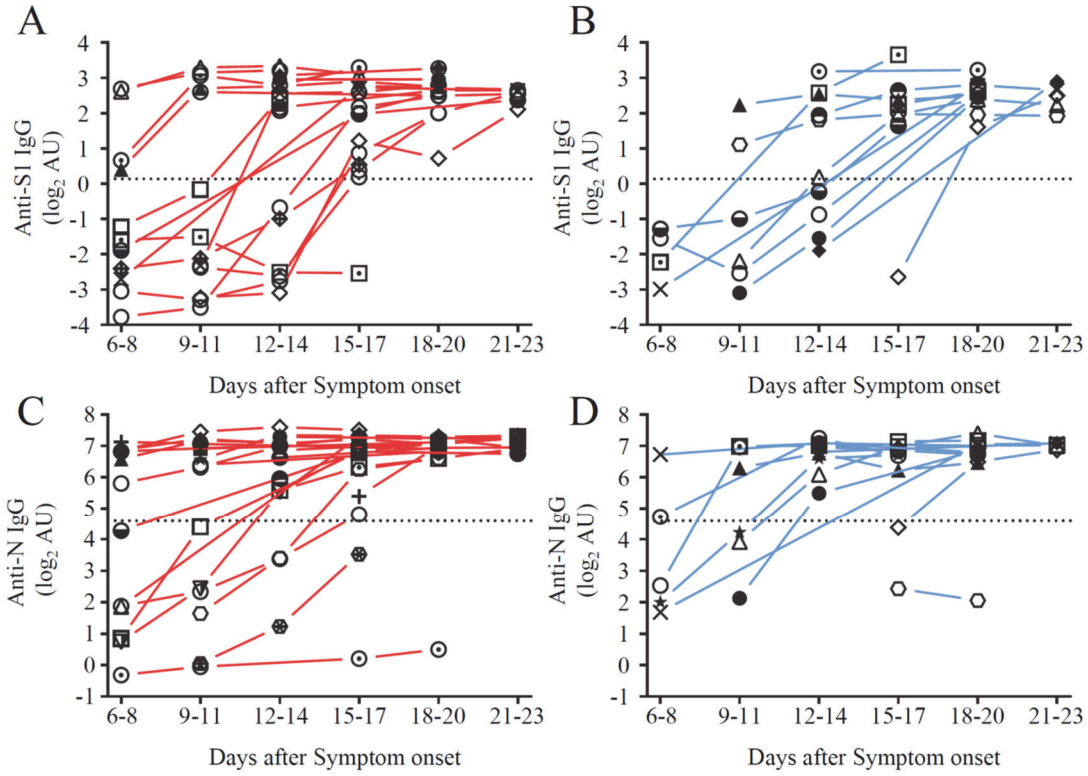

956
957
958 **Longitudinal changes in anti- SARS-CoV-2 IgG titers in severely and critically diseased**
959 **patients.**
960 Serial serum samples were collected from hospitalized COVID-19 patients and used for SARS-
961 CoV-2–specific IgG measurement. IgG responses against SARS-CoV-2 S1- and N-protein in
962 (A, C) critically (red symbols) and (B, D) severely (blue symbols) diseased patients. Dotted
963 lines represent cut-off values for commercial S1- and N- specific ELISA assays. Each symbol
964 represents the mean value of all samples which were available for each patient at the indicated
965 time range after symptom onset. There are no significant t-tests (i.e. $p>0.05$ for all
966 comparisons).
967

968 **Figure 2-figure supplement 1.**
969

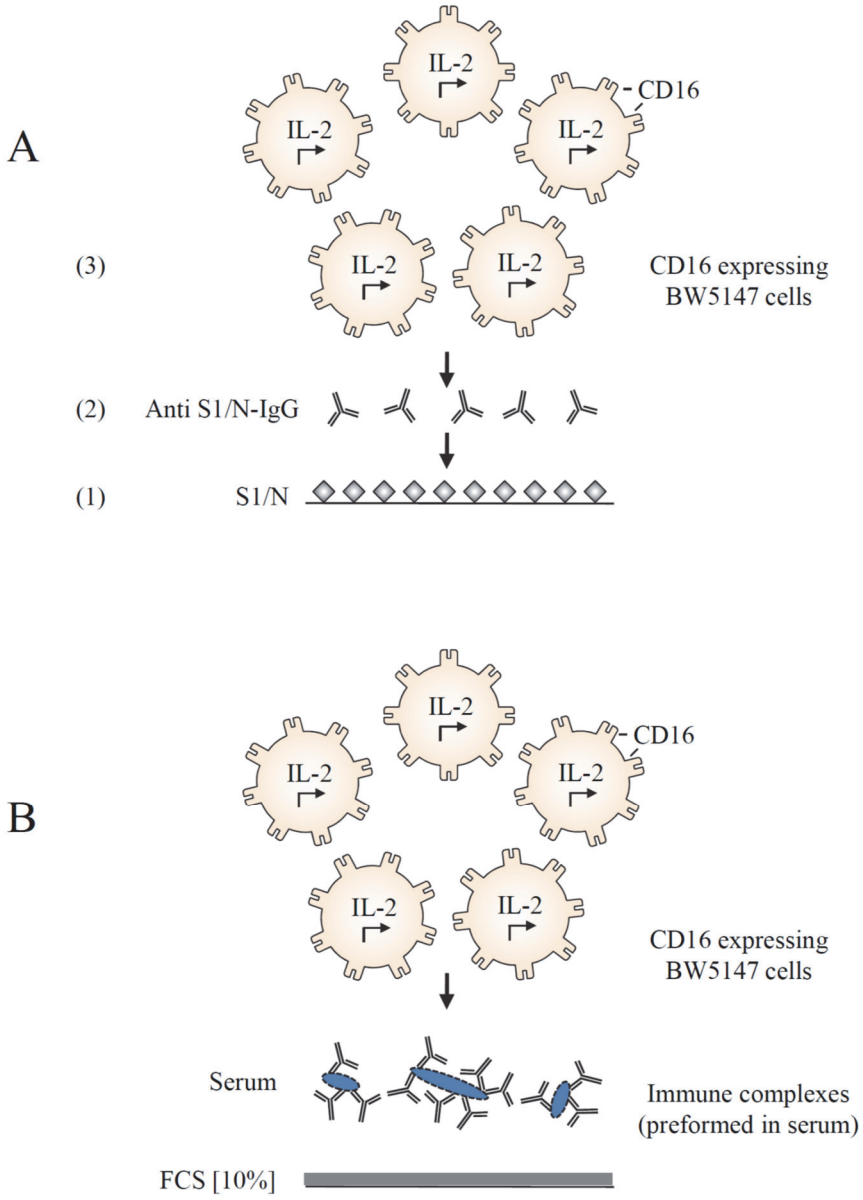

970
971
972 **Cell-based reporter assay measuring CD16 activation in response to immobilized IgG and**
973 **sICs**.
974 BW5147 reporter cells expressing chimeric human FcγRIII secrete IL-2 in response to FcγR
975 activation by A) clustered viral specific IgG binding solid-phase antigen or B) soluble ICs.
976 Solubility of sICs is achieved by pre-blocking an ELISA plate with PBS supplemented with
977 10% FCS as previously described (25, 44).
978

979 **Figure 2-figure supplement 2.**
980
981

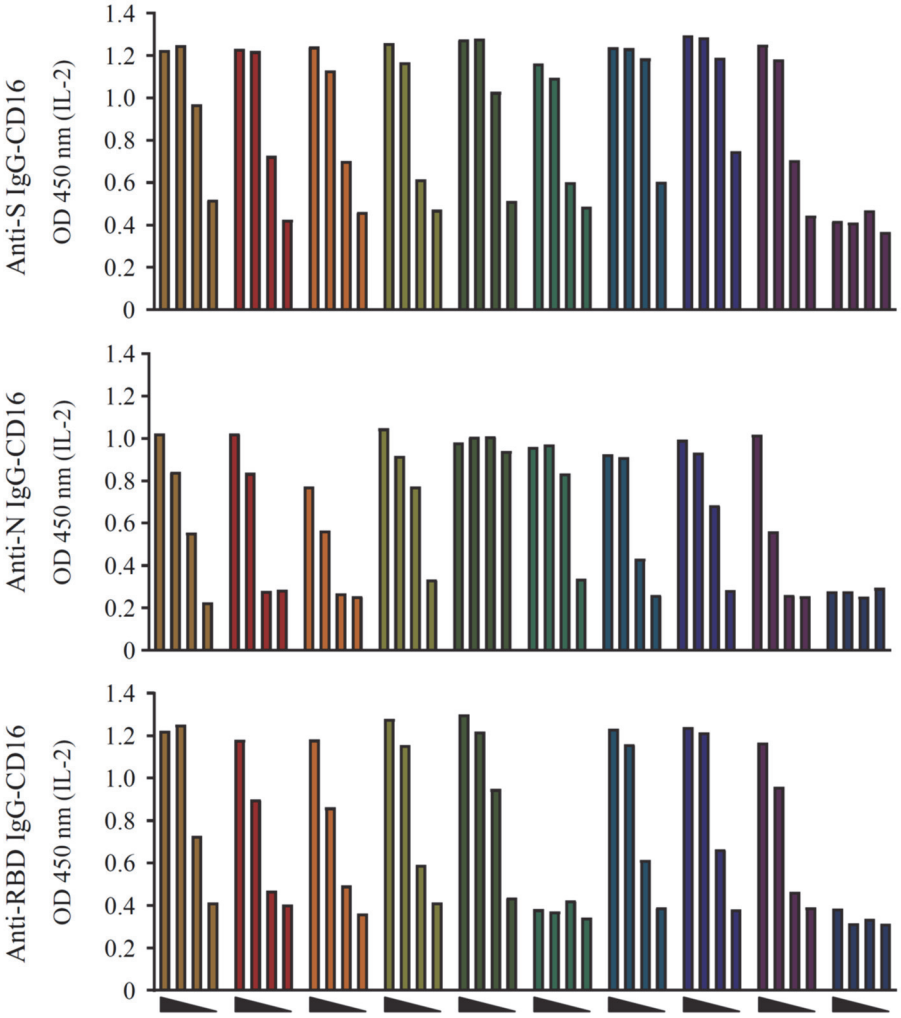

982
983
984 **Dose dependent CD16 activation by SARS-CoV-2 specific IgG.**
985 CD16 activation by A) S- , B) N- and C) RBD-specific IgG in 9 representatively selected serum
986 samples and one SARS-CoV-2 negative serum (dark blue bars). Sera were serially diluted at
987 1:20, 1:100, 1:500 and 1:2500. FcγRIII activation initiates IL-2 secretion by reporter cells,
988 which is subsequently measured via ELISA (OD 450 nm). Based on this empirical pretesting
989 all sera were thereafter tested at 1:100 and 1:500 dilutions to reach an optimal dynamic range
990 of response. The OD values obtained by the 1:500 dilutions were used for subsequent data
991 analysis.
992

993 **Figure 2-figure supplement 3.**
994
995

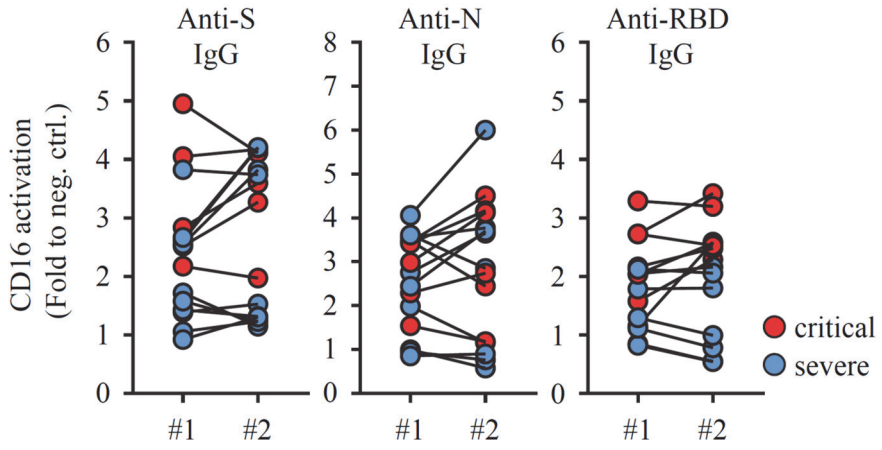

996
997
998 **Reproducibility of CD16 activation measurements by SARS-CoV-2 specific IgG.** Selected
999 sera which were available in sufficient amount from patients with critical (red symbols) or
1000 severe (blue symbols) SARS-CoV-2 infection were tested in two independent experiments to
1001 show reproducibility and consistency of results. CD16 activation by S-, N- and RBD specific
1002 IgG is shown. Statistical tests using a Kolmogorov-Smirnov test indicate no significant
1003 differences.
1004

1005 **Figure 2-figure supplement 4.**
1006

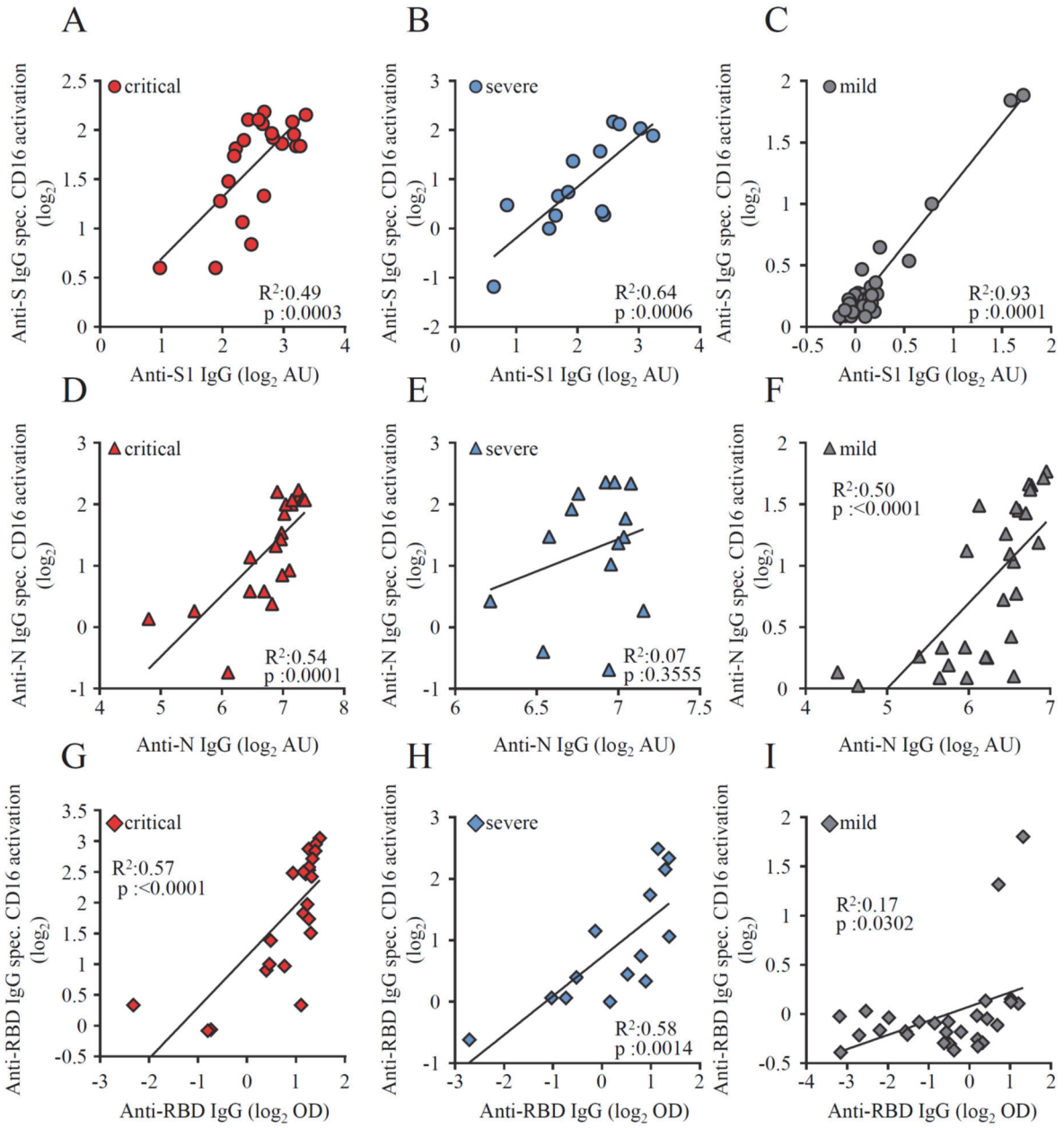

1007
1008 **Correlation of CD16 activation by virus specific IgG and ELISA levels.**
1009 Pearson's correlation coefficient was used to assess the relationship between virus–specific IgG
1010 levels and their capability to trigger CD16 activation on BW5147 reporter cells in 22 paired
1011 samples from patients with critical disease (red symbols), 14 paired samples from patients with
1012 severe disease (blue symbols) and 28 samples from patients with mild disease (grey symbols).
1013 Each dot represents the mean value obtained by the analysis of all samples available at the
1014 indicated time points. (A-C) anti-S IgG, (D-F) anti-N IgG and anti-RBD-IgG (E-I).
1015

1016 **Figure 4-figure supplement 1.**
1017
1018

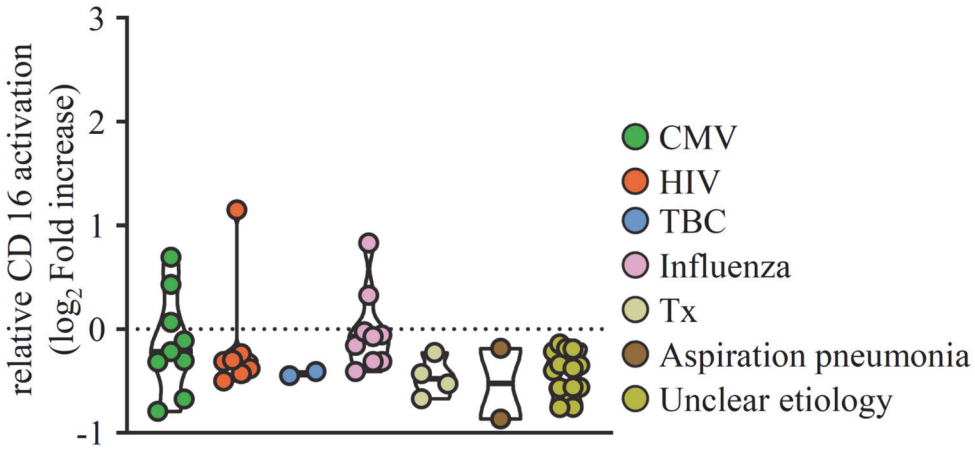

1019
1020
1021 **CD16 activation by sICs in non-COVID-19 patients with ARDS.**
1022 Serum samples from 47 patients with ARDS in response to infections of different etiology were
1023 analyzed in a cell-based reporter assay which is sensitive to sIC amount and size (25, 44). FcγR
1024 activation is shown as $\log_2$ fold change relative to negative control. Each symbol represents one
1025 sample from one patient. CMV: Cytomegalovirus reactivation under immunosuppression; HIV:
1026 HIV infection; TBC: Mycobacterium tuberculosis infection; Influenza: influenza virus
1027 infection; TX: solid organ transplantation. Solid black lines indicate the median.
1028

1029 **Figure 4-figure supplement 2.**
1030

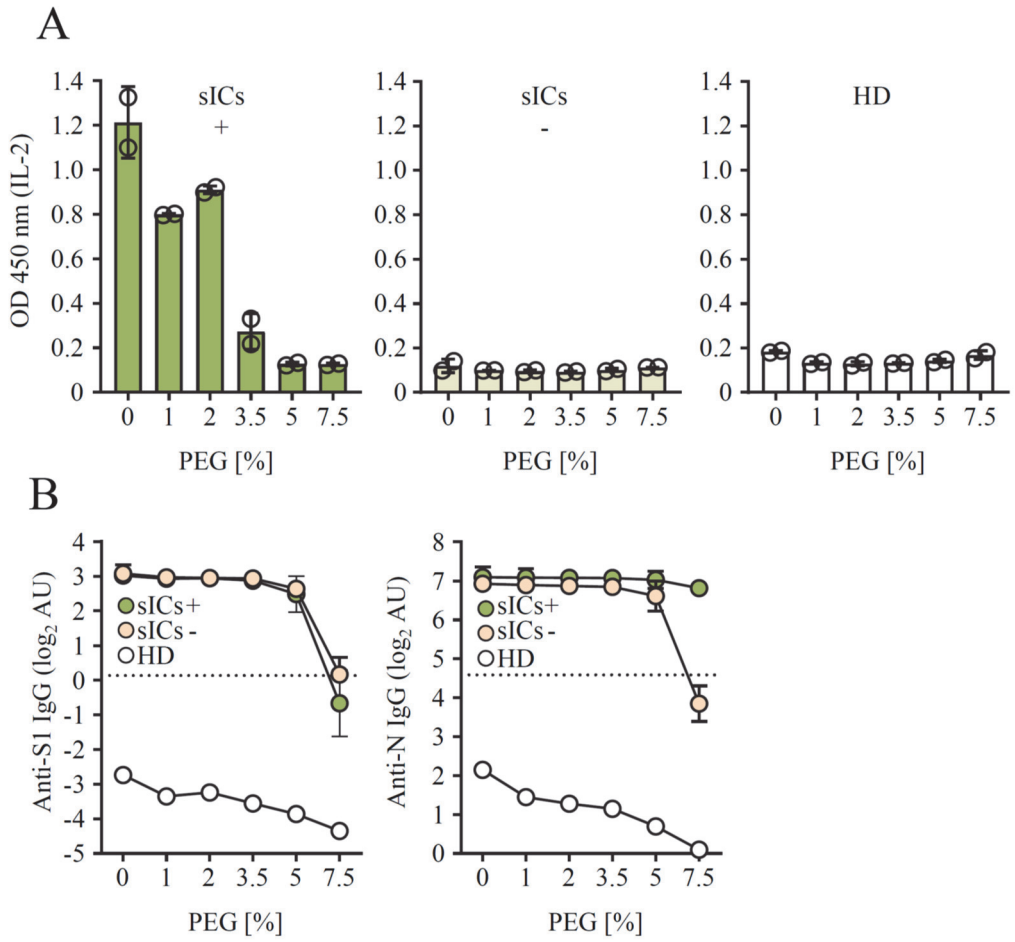

1031
1032
1033 **PEG precipitation eliminates sIC-mediated CD16 activation.**
1034 Pools of 8 sera were incubated with equal volumes of PEG8000 to reach the indicated final
1035 PEG concentrations. A) CD16 activation after PEG-precipitation in the pool supernatant,
1036 showing either high (sICs+) or no (sICs-) CD16 activation. Sera from healthy donors (HD)
1037 were included as a negative control. Activation levels are expressed as IL-2 levels (OD 450 nm)
1038 released by reporter cells. The mean and SD of two independent experiments is depicted. B)
1039 Anti SARS-CoV-2 IgG levels against S1 (left panel) or N (right panel) IgG following PEG
1040 precipitation. The mean and SD of two independent experiments (sICs+/sICs-) is depicted.
1041

1042 **Figure 4-figure supplement 3.**

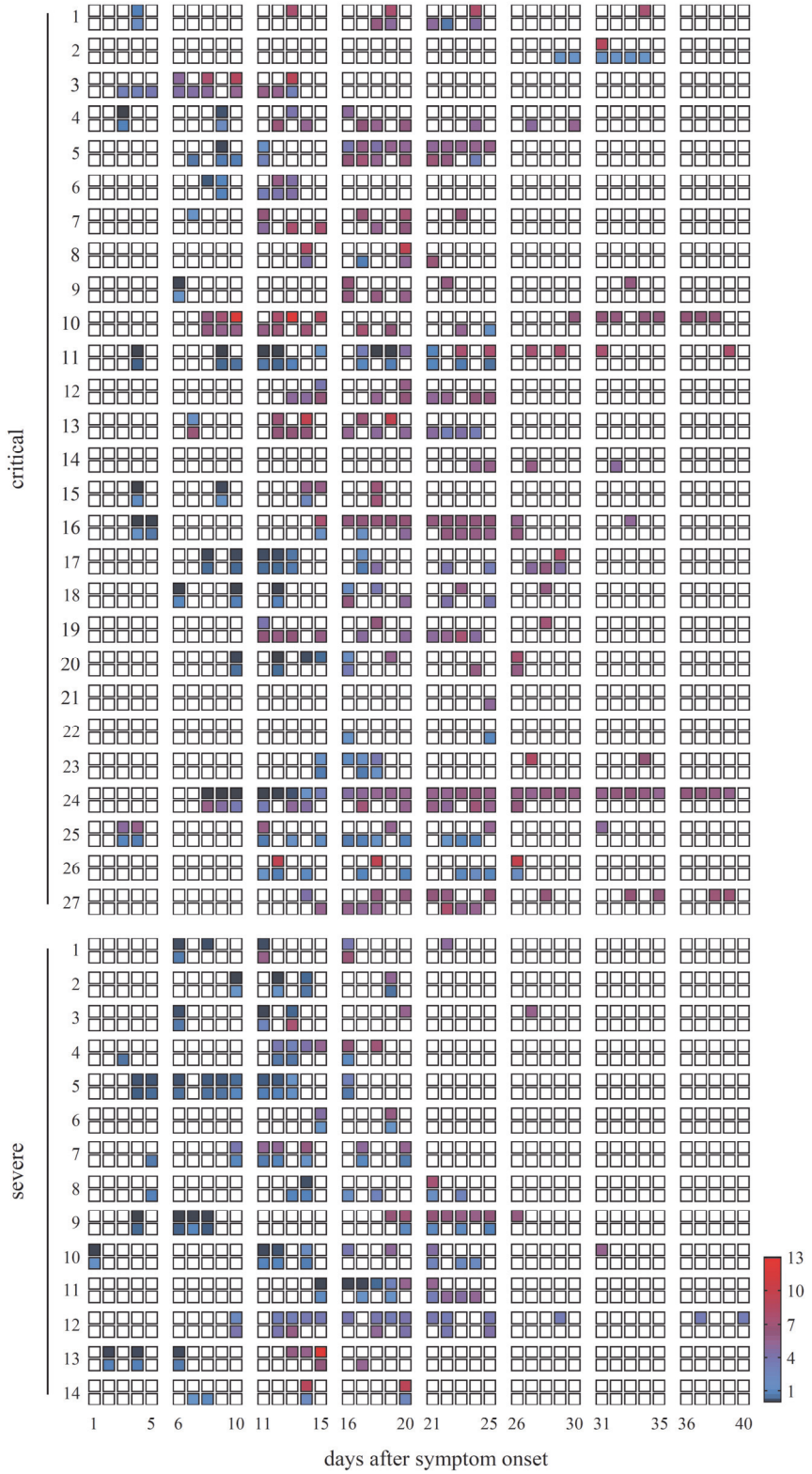

1043
1044 **Individual CD16 activation by sICs and anti-S1 ELISA IgG kinetics post symptoms onset.**
1045 Individual sera from either critically (n = 27) or severely (n = 14) diseased patients were
1046 analyzed via ELISA [AU] for anti S1-IgG (upper row) and for CD16 activation by soluble
1047 immune complexes (lower row, relative CD16 activation depicted as fold increase to the
1048 negative control) over time (1-40 days post symptom onset). White squares: not tested.
1049

1050 **Figure 4-figure supplement 4.**
1051
1052

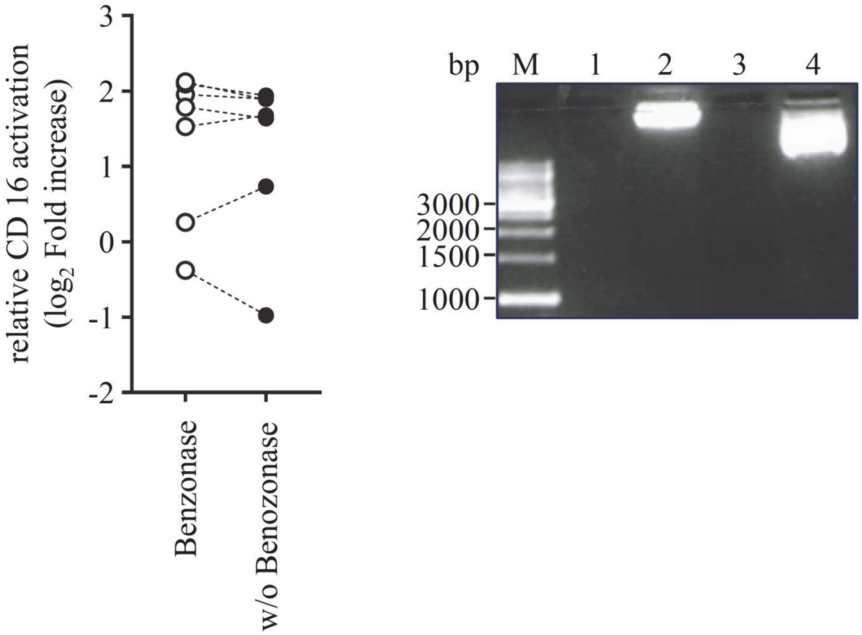

1053
1054
1055 **Benzonase treatment of sIC-reactive sera does not abolish CD16 activation.**
1056 Left panel: sIC-mediated CD16 reactivity expressed as $\log_2$ fold increase to the negative
1057 control, in serum of six individual patients before and after treatment with 250 Units of
1058 Benzonase Nuclease. Right panel: As positive control, 3 µg plasmid DNA was digested. M:
1059 1kb DNA ladder, Lane 1: benzonase digestion in the presence of human serum, lane 2: plasmid
1060 DNA w/o benzonase in the presence of human serum, lane 3: benzonase digestion in medium
1061 only and lane 4: plasmid DNA w/o benzonase in medium only.
1062

1063 **Figure 4-figure supplement 5.**
1064

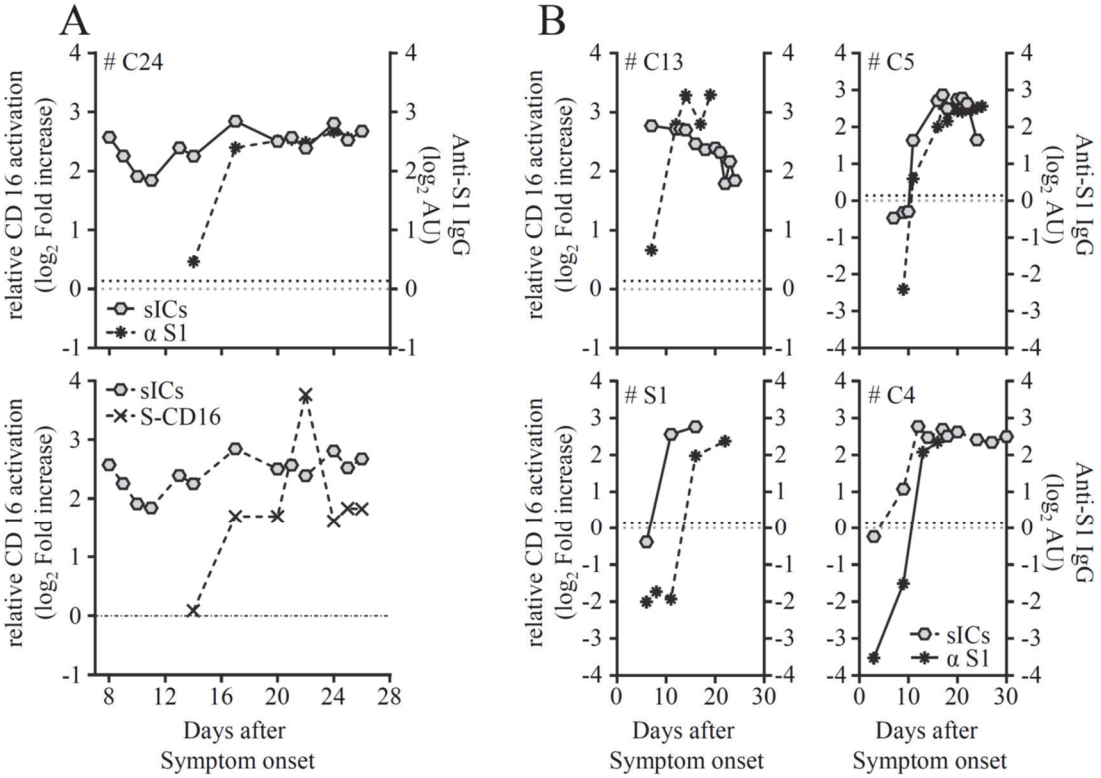

1065
1066
1067
1068 **sIC formation precedes SARS-CoV-2-IgG response.**
1069 Individual patients for which enough material was available were analyzed over time. A) CD16
1070 activation by sICs- vs. S1-ELISA (top panel) and sIC –CD16 activation vs. anti-S- CD16
1071 activation (bottom panel) in one critically ill patient, #C24. B) sIC-CD16 activation vs. S1-
1072 ELISA in four individual patients #C13, #C5, #S1 and #C4. Dashed line (black) represents
1073 commercial S1-ELISA-Cut-off level, whereas dashed line (grey) is set to 0. Individual
1074 longitudinal courses correspond to patients depicted in figure 4 supplement 3.
1075
1076
1077